

1-2013


Pliocene Sinistral Slip across the Adobe Hills, Eastern California-Western Nevada: Kinematics of Fault Slip Transfer across the Mina Deflection

Sarah Nagorsen-Rinke
Central Washington University

Jeffrey Lee
Central Washington University, jeff@geology.cwu.edu

Andrew Calvert
U.S. Geological Survey

Follow this and additional works at: <http://digitalcommons.cwu.edu/cotsfac>

 Part of the [Geology Commons](#), [Geomorphology Commons](#), and the [Tectonics and Structure Commons](#)

Recommended Citation

Nagorsen-Rinke, S., Lee, J., & Calvert, A. (2013). Pliocene sinistral slip across the Adobe Hills, eastern California-western Nevada: Kinematics of fault slip transfer across the Mina deflection. *Geosphere*, 9(1), 37-53. DOI: 10.1130/GES00825.1

This Article is brought to you for free and open access by the College of the Sciences at ScholarWorks@CWU. It has been accepted for inclusion in All Faculty Scholarship for the College of the Sciences by an authorized administrator of ScholarWorks@CWU.

In press, Geosphere

Pliocene sinistral slip across the Adobe Hills, eastern California-western Nevada: Kinematics of fault slip transfer across the Mina Deflection

Sarah Nagorsen-Rinke¹, Jeffrey Lee

Department of Geological Sciences Central Washington University, Ellensburg, WA 98926, USA

Andrew Calvert

U.S. Geological Survey, Menlo Park, CA 94025, USA

ABSTRACT

The Adobe Hills region, California-Nevada, is a faulted volcanic field located within the western Mina deflection, a right-stepping zone of faults that connects the northern Eastern California shear zone (ECSZ) to the south with the Walker Lane belt (WLB) to the north. New detailed geologic mapping, structural studies, and $^{40}\text{Ar}/^{39}\text{Ar}$ geochronology in the Adobe Hills allow us to calculate fault slip rates and test predictions for the kinematics of fault slip transfer into the Mina deflection. The Adobe Hills are dominated by Pliocene tuffaceous sandstone, basaltic lavas that yield $^{40}\text{Ar}/^{39}\text{Ar}$ ages between 3.13 ± 0.02 to 3.43 ± 0.01 Ma, and basaltic cinder cones. These Pliocene units unconformably overlie middle Miocene latite ignimbrite that yields an $^{40}\text{Ar}/^{39}\text{Ar}$ age of 11.17 ± 0.04 Ma, and Quaternary tuffaceous sands, alluvium, and lacustrine deposits cap the sequence. NNW-striking normal faults, WNW-striking dextral faults, and NE-striking sinistral faults cut all units; the NE-striking sinistral faults are the youngest and most well developed fault set. We calculate ~ 0.1 mm/yr of \sim EW-horizontal extension and NW-dextral shear since the Pliocene. The prominent NE-striking sinistral faults offset basalt ridgelines, normal fault/hanging wall intersections, a channelized basalt flow, a basalt flow edge, and a basalt flow contact a net minimum of 921 ± 184 to 1318 ± 264 m across the Adobe Hills. These measured sinistral offsets yield a minimum Pliocene sinistral fault slip rate of 0.2-0.5 mm/yr; our preferred minimum slip rate is 0.4-0.5 mm/yr. The geometry and orientation of the prominent sinistral faults are consistent with simple shear couple/clockwise block rotation within a broad dextral shear zone. Vertical axis block rotation data are needed to test this interpretation. We propose that a set of faults subparallel to Sierra Nevada-North America motion and associated releasing steps, located west of the White Mountains fault zone and east of Long Valley Caldera, transfer a portion of dextral Owens Valley fault slip northwestward onto the sinistral faults in the Adobe Hills. Dextral slip distributed across faults between the White Mountains fault zone and the Sierra Nevada and east of the Fish Lake Valley fault zone may account for the apparent discrepancy between summed long-term geologic slip rates and present day geodetic rates across the northern ECSZ. Fault slip in the Adobe Hills is part of a regional pattern of initiation and renewal of dextral, sinistral, and normal fault slip during the Pliocene that extends from latitude $\sim 40^\circ\text{N}$ to $\sim 36^\circ\text{N}$ within the ECSZ-WLB and along the western margin of the Basin and Range Province. This regional deformation episode may be related to changes in gravitational potential energy.

INTRODUCTION

¹ now at: Freeport-McMoRan Copper & Gold, P.O. Box 586, Bagdad, AZ 86321

Geologic and geodetic studies indicate that the San Andreas fault accommodates ~75–80% of relative dextral motion between the Pacific–North American plates, and the Eastern California shear zone (ECSZ)–Walker Lane belt (WLB) accommodates the remaining 20–25% (Fig. 1a) (e.g. Dokka and Travis, 1990; Dixon et al., 1995; Dixon et al., 2000; Bennett et al., 2003; Frankel et al., 2007; Lee et al., 2009a). In the northern ECSZ, dextral shear is primarily accommodated along four major, NW-striking dextral faults (Fig. 1b). These faults transfer slip northward onto several smaller, primarily ENE-striking faults within the Mina deflection, a ~125 km long by ~45 km wide deformation zone. The Mina deflection, in turn, transfers slip northward onto NW-striking dextral faults of the central WLB (Figs. 1b and 2). Thus, the Mina deflection defines an ENE-trending right-stepping relay zone within a dominantly NW-trending dextral shear zone.

Three mechanisms have been proposed to explain the fault kinematics that accommodate displacement transfer across the Mina deflection: (1) the displacement-transfer model (Fig. 3a) (Oldow, 1992; Oldow et al., 1994) in which connecting faults transfer slip via normal slip; (2) the transtensional model (Oldow, 2003) (Fig. 3b) in which oblique (sinistral) normal slip occurs along the connecting faults, and (3) the simple shear couple/fault block rotation model (Wesnousky, 2005) (Fig. 3c) in which sinistral slip occurs along the connecting faults. Geologic map relations, structural data, and seismicity in the northern ECSZ, Mina deflection, WLB, and Basin and Range province led Oldow (1992) and Oldow et al. (1994) to propose the displacement-transfer model for the Mina deflection whereby extension across NE-striking normal faults proportionally accommodates the magnitude of middle Miocene to Pliocene dextral fault slip transferred between the northern ECSZ and central WLB (Fig. 3a). Using a combination of GPS velocities, earthquake focal mechanisms, and fault-slip inversions, Oldow (2003) postulated that today instantaneous deformation across the Mina deflection region is accommodated by transtension (Fig. 3b). In this model, deformation in the western Mina deflection is characterized by extension-dominated transtension whereas the eastern part is characterized by wrench-dominated transtension. Fault geometries, sinistral offset, and paired basins at the ends of active ENE-striking faults in the Mina deflection led Wesnousky (2005) to hypothesize that during the Holocene fault blocks bounded by NE-striking sinistral faults rotated clockwise in response to NW-dextral shear across the Mina deflection (Fig. 3c). Paleomagnetic studies in the eastern Mina deflection imply clockwise rotation of 20–30° since late Miocene to early Pliocene (Petronis et al., 2007, 2009) and paleomagnetic studies in the northwestern corner of the Mina deflection indicate clockwise rotations of ~74° and ~14° since Miocene and Pliocene, respectively (Rood et al., 2011). These data suggest that the Wesnousky (2005) model is also applicable to older deformation within the Mina deflection. In contrast, geologic studies centered on Quaternary faults in the Queen Valley area did not yield evidence for recent clockwise block rotation (Lee et al., 2009b), suggesting that clockwise rotation is temporal and/or occurs in discrete zones within the Mina deflection.

The results from new detailed geologic mapping, kinematic, and $^{40}\text{Ar}/^{39}\text{Ar}$ geochronology studies completed in the Adobe Hills, western Mina deflection are reported in this paper. These data allow us to test models for fault slip transfer across the Mina deflection. From these data, we infer a portion of dextral slip along the Owens Valley fault is transferred to the sinistral faults in the Adobe Hills and that Pliocene deformation in the Adobe Hills is part of a regional Pliocene event the length of the ECSZ-WLB.

TECTONIC SETTING AND GEOLOGY OF THE ADOBE HILLS

The Adobe Hills are a ~110 km² faulted volcanic field located east of the Sierra Nevada along the eastern edge of Mono basin within the western Mina deflection (Figs. 1b, 2, and 4). The Mina deflection is underlain by Paleozoic miogeoclinal sedimentary rocks and Mesozoic volcanic rocks and granitic plutons; Neogene ignimbrite, andesite and basalt flows, tuffaceous sediments, and volcanic breccias; and Quaternary lacustrine and aeolian sediments (e.g. Gilbert et al., 1968; Krauskopf and Bateman, 1977; Oldow et al., 1992; Reheis et al., 2002; Bradley, 2005; Tincher and Stockli, 2009; Petronis et al., 2009; Oldow et al., 2009; this study). Structural, paleomagnetic, and strontium isotopic studies suggest that ENE- to NE-striking active sinistral faults within the Mina deflection followed mid-Paleozoic to Mesozoic contractional structures that, in turn, followed the morphology of an embayment in the early Paleozoic rifted continental margin of the western U.S. (Oldow et al., 1989, 2009; Tosdal et al., 2000).

Pliocene basaltic lavas and cinder cones form the Adobe Hills, interfinger with lesser early Pliocene lacustrine sediments, and overlie tilted Miocene latite ignimbrite flows, andesites, and volcanic breccias (Gilbert et al., 1968, this study). Two episodes of deformation in the Adobe Hills were noted by Gilbert et al. (1968) and in this study: (1) pre-Pliocene deformation marked by tilted and offset Miocene ignimbrite flows where the stratigraphic throw is larger than the throw of basalt flows, and (2) Pliocene to present deformation evidenced by normal, dextral, and sinistral faulting of Pliocene basalt flows. Extension and strike-slip faulting across the area has formed a complex ridge and valley morphology.

As part of a larger mapping project, Krauskopf and Bateman (1977) mapped the southern Adobe Hills at 1:62,500 scale and documented welded latite tuff, basalt flows, and basalt scoria cut by NW-, NS-, and NE-trending normal faults. Reheis et al. (2002) completed a more detailed geologic map of the western Adobe Hills that focused on Quaternary units, faults, and the Adobe Hills Spillway bedrock channel. Formation of the Adobe Hills Spillway suggests that Pleistocene faulting lowered topography and allowed southward drainage of Pleistocene Lake Russell (Reheis et al., 2002).

GEOLOGIC ROCK UNITS AND AGES

The oldest unit exposed in the Adobe Hills comprises tilted Late Miocene welded and unwelded porphyritic plagioclase + biotite ± augite-bearing latite ignimbrite (Figs. 4 and 6). Welded ignimbrite is exposed in the northern Adobe Hills at the foothills of the Excelsior Mountains, while a single outcrop of unwelded ignimbrite is exposed in the footwall of a normal fault in the southern Adobe Hills (Fig. 4). Nearly horizontal late Pliocene aphyric to phyric olivine + pyroxene- and plagioclase-bearing basalt flow cover ~80% of the Adobe Hills region and unconformably overlie tilted latite ignimbrite. The relatively high standing exposure of Mlt in the northeastern part of the field area (locality of the ⁴⁰Ar/³⁹Ar sample that yields a 11.17 ± 0.04 Ma age—see below) and the curved Mlt/Pbo contact along cross-section BB' suggest that that Mlt had paleorelief prior to eruption of the Pliocene basalt lavas (Figs. 4 and 5). Four different basalt flow units, mapped based on mineralogy and flow character, interfinger across the Adobe Hills. The source areas for these flows were not observed. Basalt flows thin to the north and northeast where they mantle older ignimbrite units (Fig. 4) (Gilbert et al., 1968). A unique channel of subrounded cobble to boulder-sized clasts of basalt lava (a channelized rubble basalt flow) containing sector-zoned pyroxene is exposed in the south-central part of the map area (Figs. 4 and 6). Lacustrine deposits and tuffaceous sandstones are locally interbedded with

lower basalt flows. Thirteen Pliocene red-weathering cinder cones overlie basalt flows. Quaternary sediments in the Adobe Hills include undifferentiated tuffaceous sands, playa deposits, basalt alluvium, landslides, and eolian deposits. Quaternary lacustrine deposits and beach gravels are concentrated in the western Adobe Hills (Reheis et al., 2002).

$^{40}\text{Ar}/^{39}\text{Ar}$ Geochronology

To constrain the age of basalt flows and faulting, and to calculate fault slip rates in the Adobe Hills, one ignimbrite sample and five basalt samples were dated using $^{40}\text{Ar}/^{39}\text{Ar}$ incremental heating techniques (Figs. 4 and 7; Table 1; Data Repository #). Analytical and data interpretation techniques are described in the data repository. Plagioclase separated from a welded latite ignimbrite from the northeastern Adobe Hills, unit Mlt (sample AH09-41), yields an $^{40}\text{Ar}/^{39}\text{Ar}$ plateau age of 11.17 ± 0.04 Ma. Groundmass concentrates from samples of dense basalt flow interiors yield either plateau ages or decreasing age spectra due to ^{39}Ar recoil (Turner and Cadogan, 1974; Onstott et al., 1995). Recoil model ages for these recoil-affected samples are calculated by incorporating age dispersion into the weighted mean age error, and are interpreted as the most reliable ages. The oldest dated basalt flow, unit Pbc (sample AH09-42), collected on the same ridge as the dated welded ignimbrite, yields a plateau age of 3.43 ± 0.01 Ma. Two unit Pbo basalt flows were dated, one from the top of a normal fault bounded ridge (sample AH08-35) yields a plateau age of 3.28 ± 0.03 Ma and the other from the base of the same ridge (sample AH09-201) yields a recoil model age of 3.39 ± 0.03 Ma. The channelized, rubble basalt flow, unit Pbr (sample AH08-19b), offset along a sinistral fault in the south-central Adobe Hills, yields an $^{40}\text{Ar}/^{39}\text{Ar}$ plateau age of 3.20 ± 0.03 Ma. The youngest dated basalt flow, collected from unit Pbc at the top of a sinistral fault scarp in the northeastern Adobe Hills (sample AH08-33), yields a recoil model age of 3.13 ± 0.02 Ma. Our geochronologic data suggests that the basalt flows exposed across the Adobe Hills were emplaced over a short time period, <400 kyr.

FAULTS IN THE ADOBE HILLS

NNW-striking normal faults, WNW-striking dextral faults, and NE-striking sinistral faults cut and offset Miocene ignimbrite flows, Pliocene sediments and basalt flows, and some Pliocene cinder cones (Figs. 5 and 8). Fault scarps are primarily characterized by near-vertical faces that expose flow features within basalt, and slickenlines are rare. Seismicity in the area indicates that faults are still active (Ryall and Priestly, 1975; Rogers et al., 1991; dePolo et al., 1993), however ash fallout and wind-blown volcanic glass, ash, and small lithics from Mono and Inyo Craters obscure latest Pleistocene and Holocene fault scarps, if developed. Reheis et al. (2002) note that some fresh fault scarps are exposed in the western Adobe Hills.

Fault Geometry and Geomorphology

Although a small data set, tilted bedding and flow foliation measurements within Mlt along with paleorelief on Mlt suggest an episode of deformation prior to eruption of the Pliocene basalt lavas. Within the central WLB and northern ECSZ, map, structural, paleomagnetic, and geochronologic data reveal late Miocene EW-extension, dextral slip, and vertical axis rotations (e.g. Dilles and Gans, 1995; Stockli et al., 2003; Tincher and Stockli, 2009; Rood et al., 2011) indicating that the region underwent deformation at this time. This deformation episode combined with erosion likely resulted in the paleorelief along the unconformity between Mlt and

the overlying Pliocene lavas (Figs. 4 and 5). However, because of the limited exposure of Mlt, the nature of this late Miocene deformation in the Adobe Hills area is not known.

The oldest set of faults are NS- to NW-striking curvilinear to straight normal faults that range from ~0.2 to 2 km in length and 10 to 130 m in fault scarp height (Figs. 4, 5, and 8). Evidence for normal faulting includes linear to moderately curved valleys in conjunction with vertically offset basalt flows and exposed Miocene ignimbrite flows and Pliocene sandstone in the footwall of faults. In the southern Adobe Hills, normal faults strike northwest near the trace of fault 3 and strike north with increasing distance away from this fault (Figs. 4 and 8). Some normal faults in the Adobe Hills are sinistrally or dextrally offset, while others define left-steps along sinistral faults (Figs. 4, 8, and 9). All normal faults displace late Pliocene basalt flows and older units; therefore, all normal faulting post-dates Pliocene basalt volcanism, and mostly pre-dates sinistral faulting.

A few NW-striking, right lateral faults, exposed near the southern boundary of the Adobe Hills (Figs. 4 and 8), are the least abundant fault type. These faults offset normal faults, but not sinistral faults; therefore, dextral faulting occurred after normal faulting and before sinistral faulting.

The youngest and most prominent faults in the Adobe Hills comprise five major and numerous minor NE-striking near-vertical sinistral faults, ranging from 6 to 12 km in fault trace length and 10s of cm to ~100 m in scarp height (Figs. 4, 5, and 8). Sinistral faults traverse nearly the entire field area, are well defined in the central, northern, and eastern areas, and become more diffuse towards the south and southwest where they are represented by several en echelon short fault strands. Sinistral faults are characterized by linear valleys, alternating scarp-facing directions along fault strike, left-stepping extensional (Fig. 9) and right-stepping compressional stepovers, and sinistrally offset normal fault/hanging wall surface intersections, ridgelines, contacts, and channelized flows (Figs. 4, 8, and 10). Linear valleys in conjunction with fault scarps 10's of cm to 100 m in height along the sinistral fault traces may indicate these faults also accommodated a small component of extension in addition to the dominant sinistral offset. However, two field observations imply that the magnitude of extension is likely negligible: (a) fault traces are linear and cross-cut topography suggesting near vertical fault dips (80-90°) and (b) the fault scarps change facing direction along strike suggesting this geometry is the result of sinistral fault slip along a near vertical fault that juxtaposed topographic lows against topographic highs.

Magnitude of Fault Slip and Fault Slip Rates

The NS- to NW-striking normal faults in the south-southwestern Adobe Hills suggest this area experienced ~EW-directed extension over a relatively short period of geologic time—after late Pliocene basalt emplacement, but before Pliocene sinistral faulting began. In the absence of vertically displaced marker beds, we estimate a minimum ~EW-horizontal extension magnitude along transect *A* (Fig. 8) using the height of exposed fault scarps and assuming a fault dip of 60°. The transect records a minimum vertical offset of 495 m, which along with the range of basalt ages of 3.13 ± 0.02 to 3.43 ± 0.01 Ma, yields a minimum horizontal extension rate of ~0.1 mm/yr. The rate of ~EW-extension could be an order of magnitude higher if this extensional episode, bracketed between basalt emplacement and onset of sinistral faulting, were a few hundred thousand years.

Dextral faults are limited to the southern Adobe Hills and offset normal faults, but do not offset sinistral faults. One NW-striking dextral fault in the southern Adobe Hills offsets a normal fault/hanging wall surface intersection lineation and Pbo basalt ridgeline by 281 ± 42 m. This offset measurement, combined with an $^{40}\text{Ar}/^{39}\text{Ar}$ basalt age range of 3.28 ± 0.03 to 3.39 ± 0.03 Ma for unit Pbo, yields a minimum dextral slip rate of ~ 0.1 mm/yr. Like the EW-extension rate, the rate of dextral shear could be an order of magnitude higher if this deformation episode, bracketed between basalt emplacement and onset of sinistral faulting, were a few hundred thousand years.

The youngest, longest, and most prominent set of faults exposed across the field area are five major NE-SW striking sinistral fault zones. Measurable sinistral offset magnitudes along individual fault strands range from 151–527 m and calculated minimum slip rates along individual fault zones range from 0.1–0.2 mm/yr (Figs. 4, 8, and 10; Table 2).

Fault 1, located in the southeastern Adobe Hills, offsets a Pbc basalt flow edge and a contact between a scoria deposit (Pbs) and underlying Pbo basalt flow 225 ± 33 m and 268 ± 54 m, respectively. The latter may be an apparent offset because the contact between Pbs and Pbo is shallow. Fault offset magnitude, combined with an $^{40}\text{Ar}/^{39}\text{Ar}$ basalt age range of 3.28 ± 0.03 to 3.39 ± 0.03 Ma, yields a minimum sinistral slip rate of ~ 0.1 mm/yr for this fault (Table 2). This slip rate is similar or less than rates along the other sinistral faults within the Adobe Hills (see below), which suggests to us that the measured apparent 268 m sinistral offset of the Pbs/Pbo contact is reasonably accurate.

Evidence for the magnitude of sinistral offset along fault 2 is exposed along its northeastern trace and a set of splays along its southwestern trace. In the northeast, the fault consists of two splays that sinistrally offset units Pbc and Pbo, and the intersection line defined by a NE-dipping normal fault and the subhorizontal surface of its hanging wall basin a total of 695 ± 139 m (Figs. 4, 8, and 10a). This offset measurement, combined with ages for the top and bottom of a nearby offset Pbc basalt flows of 3.13 ± 0.02 Ma and 3.43 ± 0.01 Ma, yields a minimum sinistral slip rate of 0.2–0.3 mm/yr (Table 2). A zone of three small (0.4 to 1 km long) subparallel sinistral faults offset units Pbc and Pb along the southwestern segment of fault 2 (Figs. 4, 8, and 10b). Here, the total offset of the intersection line between normal faults and surface of hanging wall basins, and a basalt ridge-line across the three faults is 523 ± 78 m. This offset measurement, combined with a basalt $^{40}\text{Ar}/^{39}\text{Ar}$ age range of 3.13 ± 0.02 to 3.43 ± 0.01 Ma, yields a minimum slip rate of 0.1–0.2 mm/yr (Table 2).

Evidence for magnitude of sinistral offset along the trace of fault 3 is exposed towards its southwestern end (Figs. 4, 8, and 10c). Fault 3 sinistrally offsets a distinct channelized rubble basalt flow (unit Pbr) 527 ± 79 m. Combining this offset with an $^{40}\text{Ar}/^{39}\text{Ar}$ age of 3.20 ± 0.03 Ma for this basalt unit yields a minimum late Pliocene sinistral slip rate of ~ 0.2 mm/yr (Table 2).

We did not observe offset geologic markers along sinistral faults 4 and 5 (Fig. 4). However, the geomorphic expression for these two faults is as well developed as fault 1, but somewhat less well developed compared to faults 2 and 3. We infer, therefore, that the Pliocene sinistral slip rate along both faults 4 and 5 is ~ 0.1 mm/yr.

Because we can measure offsets on only three out of the five major sinistral fault zones, our calculated net sinistral offsets across transects *B* and *C* of 921 ± 184 m and 1318 ± 264 m (Fig. 8), respectively, are minimum estimates. Combining these measurements with the age range of basalt flows of 3.13 ± 0.02 Ma to 3.43 ± 0.01 Ma yields a minimum net sinistral slip rate of between 0.2–0.5 mm/yr. If our assessments are valid that the expression of sinistral faults 4 and 5

is similar to fault 1, but less so than faults 2 and 3, and that each records fault slip rates of ~ 0.1 mm/yr, then we suggest that 0.4-0.5 mm/yr is a reasonable estimate for a minimum Pliocene sinistral slip rate across the Adobe Hills.

DISCUSSION

Mechanisms of Fault Slip Transfer Across the Mina Deflection

The Adobe Hills area, located in the southwestern part of the Mina deflection, accommodated late Pliocene to Recent fault slip. Five geomorphically prominent NE-striking sinistral fault zones dominate the region. Fault slip to a lesser extent also occurred along older NS- to NNW-striking normal faults and NW-striking dextral faults. All faults cut Pliocene basalts and older units, and likely Quaternary deposits (Fig. 4). We calculate a minimum Pliocene sinistral fault slip rate of 0.2-0.5 mm/yr across the Adobe Hills; our preferred minimum sinistral slip rate is 0.4-0.5 mm/yr. Calculated minimum Pliocene WNW-EES extension rates across older normal faults and NW-dextral fault slip rates are both ~ 0.1 mm/yr.

The Mina deflection defines a right-step between the NW-striking dextral faults in the northern ECSZ and the NW-striking dextral faults exposed in the central WLB (Figs. 1b and 2). The prominent NE-striking sinistral faults in the Adobe Hills are exposed in the southwestern part of this right step. A similar geometric configuration exists in the Carson domain, central WLB (see gray shaded area southeast of Reno; Fig. 1b), a $\sim 2,420$ km² zone of NE-striking sinistral faults that transfers dextral slip between NW-striking Pyramid Lake, Warm Springs Valley, and Honey Lake dextral faults exposed to the north and NW-striking Gumdrop Hill, Benton Springs, and Petrified Springs dextral faults exposed to the south (Cashman and Fontaine, 2000) (Fig. 1b). Paleomagnetic data from the Carson domain indicate dextral fault slip transfer has occurred via $\sim 55^\circ$ to $\sim 11^\circ$ of Miocene to Pliocene clockwise block rotation (Cashman and Fontaine, 2000).

Clockwise rotation of blocks has been also documented in the eastern, southeastern, and northwestern parts of the Mina deflection. In the Candelaria Hills, eastern Mina deflection, and the Silver Peak area, to the southeast of the Mina deflection (Fig. 1b), Petronis et al. (2009, 2007) documented block rotations of $20-30^\circ$ and $20-25^\circ$ since the late Miocene to early Pliocene. Similarly, in the Bodie Hills region northwest of Mono Lake Basin and to the northwest of the Mina deflection (Fig. 1b), paleomagnetic studies indicate clockwise rotations of $\sim 74^\circ$ and $\sim 14^\circ$ since the Miocene and Pliocene, respectively (Rood et al., 2011).

NE-striking right-steps between dextral systems are documented elsewhere in the northern ECSZ and include the Queen Valley, Deep Springs, Towne Pass, and numerous other normal faults that transfer dextral slip from the Owens Valley and Hunter Mountain–Panamint Valley fault zones to the Death Valley–Fish Lake Valley fault zone (Figs. 1b and 2) (e.g. Lee et al., 2009b; Lee et al., 2001; Reheis and Dixon, 1996; Sternlof, 1988). These faults are unlike those in the Adobe Hills area and Carson domain in that they act as right-stepping releasing bends and transfer dextral fault slip via normal faulting. None of these faults show geologic evidence (e.g. oblique slip) for vertical axis rotation.

Three fault kinematic models have been proposed to explain the mechanisms by which dextral fault slip is transferred from the northern ECSZ through the Mina deflection and into the central WLB. Each model was developed for a particular time period and, taken together, imply that the mechanism of fault slip transfer has changed through time. In the displacement-transfer model, curved NE-striking normal faults in the Mina deflection accommodated the magnitude of

dextral fault slip transfer from the northern ECSZ to the central WLB during the middle Miocene to Pliocene (Fig. 3a) (Oldow, 1992; Oldow et al., 1994). In the Adobe Hills region, the N- to NW-strike of normal faults do not fit the NE-striking geometry required of this model and the NE-striking faults record sinistral slip with little or no normal slip. Thus, this model is not applicable to this part of the Mina deflection.

In the transtensional model, instantaneous fault slip today across the western Mina deflection is characterized by extension-dominated transtension, and across the eastern part by wrench-dominated transtension (Oldow, 2003) (Fig. 3b). In the Adobe Hills, NNW-striking normal faults are exposed in the southwestern part of the Adobe Hills, accommodate a minimum of ~ 0.1 mm/yr of horizontal extension—a rate smaller than the minimum sinistral fault slip rate (although see note above regarding the possibility of an order of magnitude higher extension rate)—and are older than the sinistral faults. Thus, in the Adobe Hills extensional and transcurrent deformation episodes were partitioned in space and time, and transcurrent fault slip was the dominant deformation style. We conclude that the extension-dominated transtension model proposed for instantaneous fault slip transfer today across the western Mina deflection was not the style of deformation that resulted in the types and geometries of faults exposed across the Adobe Hills region.

In the simple shear couple/fault block rotation model (Wesnousky, 2005) (Fig. 3c), ENE-striking sinistral faults spaced 10 km apart in the Mina deflection rotated $\sim 20\text{--}30^\circ$ clockwise during the Holocene from an original orientation near perpendicular to dextral faults of the northern ECSZ and central WLB. Paired basins on the NE and SW ends of sinistral faults may have formed as a consequence of extension at the tips of sinistral faults during rotation between bounding NW-striking dextral faults (Wesnousky, 2005). Sinistral faults in the Adobe Hills spaced 0.3–1 km apart strike roughly N40E, while major sinistral faults in the eastern Mina deflection strike more easterly (N60E to N90E). Furthermore, none of the sinistral faults in the Adobe Hills are single, through-going structures; rather, they are characterized by en echelon segments and splays. With continued displacement, the en echelon fault segments and splays might coalesce into single, through-going sinistral faults (e.g. Wesnousky, 2005). Some of the sinistral faults centered on the Adobe Hills exhibit paired basins, consistent with the model. For example, north of Huntoon Creek, sinistral fault scarps along faults 2, 3, and 4 generally face northwest and basins are developed on the northwest side of the fault traces (Figs. 4 and 8), as predicted by the model (Fig. 3c). However, our reconnaissance mapping suggests the northeastern fault tips are beyond the field area. At the southern tips of sinistral faults 2 and 4, fault scarps face southeast and basins are developed on the southeast side of the fault traces, as also predicted by the model (Fig. 3c). The southern tip of fault 3 faces northwest with a basin on its northwest side in contrast to faults 2 and 4. Thus, sinistral faults in the Adobe Hills possess some of the features predicted by the fault block rotation model, but not all. The complexity of fault geometries in the Adobe Hills (Figs. 4 and 8) suggest that, if fault block rotation occurred, then it likely occurred at a scale of fault blocks spaced 0.3–1 km apart as compared to more widely spaced (~ 10 km) large fault blocks bounded by the primary sinistral faults of the Mina deflection (Figs. 1a and 2).

Although exposed fault striations are rare along the sinistral faults in the Adobe Hills, the geometry and orientation of these faults with respect to the NW-striking dextral faults that define the northern ECSZ to the south and the central WBL to the north, are consistent with the simple shear couple/fault block rotation model (e.g. McKenzie and Jackson, 1983, 1986; Wesnousky,

2005) (Fig. 3c). It is therefore likely that fault blocks bounded by sinistral faults in the Adobe Hills fault zone rotated clockwise during fault slip. Additional data are needed to characterize fault kinematics, particularly vertical axis fault block rotation data from paleomagnetic studies, to test the mechanisms of fault slip transfer across the western Mina deflection.

Kinematics of Fault Slip Transfer into the Western Mina Deflection

Field-based studies of faults in Queen Valley, located in southwestern part of the Mina deflection (Figs. 1a and 2), led Lee et al. (2009b) to propose a kinematic fault slip model whereby 0.8–0.4 mm/yr of Pliocene to Pleistocene dextral fault slip was transferred northward from the White Mountains fault zone onto sinistral faults in the western Mina deflection via the dextral Coyote Springs fault (Fig. 2). The Adobe Hills, across which we have documented a minimum late Pliocene sinistral slip rate of 0.4–0.5 mm/yr, is located to the west of the northwest projection of the Coyote Springs fault (Fig. 2). The Pizona Springs area, located to the east and southeast of the Adobe Hills (Fig. 2), is located at the northwestern tip of the Coyote Springs fault. In this area, geomorphically prominent sinistral faults are subparallel to and as well developed as the ones we have documented in the Adobe Hills, and cut basalt and andesite flows (J. Lee, unpublished mapping; E. Hogan, unpublished mapping) (Fig. 2). Thus, we speculate that the Pliocene sinistral slip rate along each sinistral fault in the Pizona Springs area is ~0.1–0.2 mm/yr, the same as we have documented along sinistral faults in the Adobe Hills. If the predicted ~0.8–0.4 mm/yr fault slip transfer rate is correct, and the Coyote Springs fault abuts these sinistral faults, then the Pizona Springs area of the western Mina deflection accommodated transfer of dextral slip from the White Mountains fault zone; those in the Adobe Hills did not.

This raises the question: what system of faults in the northern part of the ECSZ transfers slip onto the sinistral faults of the Adobe Hills? Based on the orientation of dextral and normal faults with respect to small circles about the Sierra Nevada–North American Euler pole and kinematic inversions of earthquake focal mechanisms, Unruh et al. (2003) postulated that normal faults in this region were the result of plate-boundary-driven NW translation of the Sierra Nevada microplate. Furthermore, Unruh et al. (2003) noted that major grabens along the northeastern flank of the Sierra Nevada define a westward stepping fault array, and thus a releasing step with respect to Sierra Nevada–North American motion. Following Unruh et al.'s (2003) ideas, we suggest that the normal faults exposed within the Volcanic Tableland extending northward into the southern part of Adobe Valley, west of the White Mountains fault zone, play a similar role and transfer dextral fault slip northward into the Adobe Hills (Figs. 2 and 11).

The Volcanic Tableland is characterized by east- and west-facing normal faults, with an average strike of N10–20°W (Pinter, 1995), which cut the 758.9 ± 1.8 ka Bishop Tuff (Sarna-Wojcicki et al., 2000). These faults strike ~25–35° clockwise relative to motion of the Sierra Nevada microplate with respect to a fixed North American plate (Dixon et al., 2000), thus defining a releasing step. Locally within the Volcanic Tableland, normal faults curve westward defining zones of en echelon faults that trend ~315°, subparallel to the Sierra Nevada–North American motion. This geometric configuration suggests that these faults accommodate dextral slip. The normal faults extend northward and east of the Long Valley caldera into the Benton Range, Black Mountain, and the southern part of Adobe Valley (Krauskopf and Bateman, 1977; Rinehart and Ross, 1957; Crowder and Sheridan, 1972; Bateman, 1965; Nevin, 1963) (Figs. 2 and 11).

Across the southern part of the Volcanic Tableland, Pinter (1995) estimated 144-332 m of Pleistocene horizontal extension. This extension estimate combined with the age of the Bishop Tuff yields 0.2-0.4 mm/yr of ~N75E–S75W-extension since its eruption. To the north, across the southern part of Adobe Valley including Black Mountain and the Benton Range, Nevin (1963) estimated ~1.94 km of horizontal extension. Here, NNW-striking normal faults cut Pliocene basalt flows that can be traced continuously into the Adobe Hills (Krauskopf and Bateman, 1977). This map relation suggests the basalt flows exposed in the Black Mountain and the Benton Range are probably the same age as the ones we dated. Combining that age range with the magnitude of horizontal extension yields ~0.6 mm/yr of ~ENE–WSW-extension across the southern part of Adobe Valley.

The simple fault map in Figure 11 illustrates how normal faults straddling the southern part of Adobe Valley, which accommodate ~EW-extension, transfer slip onto the sinistral faults we have documented. These NNW-striking normal faults accommodated ~0.6 mm/yr of ENE-WSW extension since the Pliocene. This slip was transferred to NW-striking oblique-slip faults that bound the eastern margin of Adobe Valley and as well as likely in the valley, although the latter are now mostly buried. Based on the geometric relationships, slip along this NW-striking fault system is predicted to be oblique, dominantly normal (~0.5 mm/yr) with a lesser component of dextral slip (~0.3 mm/yr). The normal component is nearly parallel to the sinistral faults we mapped in the Adobe Hills, thus predicting ~0.5-0.6 mm/yr of sinistral slip in the Adobe Hills since the Pliocene, consistent with our preferred minimum sinistral slip rate of 0.4-0.5 mm/yr. The dextral component is almost perpendicular to the sinistral faults in the Adobe Hills, thus our simple kinematic model predicts ~0.2 mm/yr of extension across the sinistral faults. However, as discussed above, there is little, if any, extension accommodated along these faults. We suggest that the predicted 0.2 mm/yr NW-SE extensional component of slip was partitioned onto the ~NS-striking normal faults that have been documented throughout this region by our work and in the far western Adobe Hills (Reheis et al., 2002) as well as onto the NW-striking dextral faults we documented.

The Pliocene ENE-WSW horizontal extensional rate across the Black Mountain and Benton Range could be closer to 0.4 mm/yr, the calculated ENE-WSW horizontal extensional rate across southern Volcanic Tableland if: (a) the basalt flows exposed in the Black Mountain and the Benton Range are somewhat older than the flows we studied in the Adobe Hills, (b) all of the Pleistocene ENE-WSW horizontal extension across the southern part of the Volcanic Tableland was transferred to normal faults exposed in the Black Mountain and Benton Range, and (c) fault slip rates have been constant through time. Using the same geometric relationships described above, the implications for slip rates in the Adobe Hills for a 0.4 mm/yr horizontal extension rate across Black Mountain and the Benton Range are 0.3-0.4 mm/yr of extension and 0.1-0.2 mm/yr of dextral slip along the NW-striking oblique slip faults in the eastern part of Adobe Valley and 0.3-0.4 mm/yr of sinistral slip and 0.1-0.2 of extension across the NE-striking sinistral faults in the Adobe Hills. As stated above, we suggest that the predicted 0.1-0.2 mm/yr NW-SE extensional component of slip across the NE-striking sinistral faults was partitioned onto the ~NS-striking normal faults and NW-striking dextral faults exposed in the Adobe Hills region.

Figures 2 and 11 show a series of releasing steps between the dextral Owens Valley fault and faults bounding the eastern edge of Adobe Valley. The set of releasing steps from the northern end of the Owens Valley fault northward to Bishop indicate that dextral slip along the Owens Valley fault is transferred to both the White Mountains fault zone (Reheis and Dixon, 1996;

Kirby et al., 2006, 2008; Sheehan, 2007) and the Volcanic Tableland. Releasing steps are common elsewhere within the dextral ECSZ-WLB, and have been described across the Towne Pass, Deep Springs, and Queen Valley normal faults and the Death Valley, Panamint Valley, and Saline Valley pull-apart basins (Lee et al., 2001; Lee et al., 2009a, b; Oswald and Wesnousky, 2002; Stockli et al., 2000; Burchfiel et al., 1987; Burchfiel and Stewart, 1966). Fault slip transfer via releasing bends or extensional step-overs is also common, at a range of scales, within strike-slip fault systems worldwide (e.g. Cunningham and Mann, 2007) and have been documented in analog models (e.g. McClay and Dooley, 1995). Thus, we are not surprised that a set of releasing steps, of varying scales, occur within the northern ECSZ and transfer slip from one major structure or set of structures to another.

Regional Tectonics

Geologic vs. Geodetic Rates

The results from our studies in the Adobe Hills provide insight into whether there is an apparent discrepancy between summed geologic slip rates vs. geodetic rates across the northern ECSZ (cf. Lee et al., 2009a; Frankel et al., 2007; Kirby et al., 2006; Bennett et al., 2003) and, combined with the results of several other studies along the eastern side Sierra Nevada, the forces that drive deformation along the western boundary of the Basin and Range Province. At the latitude of $\sim 36.5^\circ$, cumulative long-term geologic dextral slip rates across the Owens Valley, Hunter Mountain, northern Death Valley, and State Line faults yield a net dextral slip rate that is the same, within error, to geodetic estimates (cf. Lee et al., 2009a; Bennett et al., 2003). In contrast, at latitude of $\sim 37.5^\circ$ there is an apparent discrepancy between the summed late Pleistocene dextral geologic slip rates along the Fish Lake Valley and White Mountains dextral fault zones (Frankel et al., 2007; Kirby et al., 2006), which at 2.4-3.9 mm/yr (Frankel et al., 2007) is less than geodetic rates, assuming that the geodetic dextral strain rate for the northern ECSZ at $\sim 36.5^\circ$ latitude (9.3 ± 0.2 mm/yr) (Bennett et al., 2003) and central WLB at 38-39° latitude (~ 10 mm/yr) (Hammond and Thatcher, 2007) are the same as 37.5° . This apparent discrepancy suggests that either (a) additional dextral slip was accommodated on structures to the east of these two faults, distributed across Owens Valley, and/or west of the White Mountains fault zone (Frankel et al., 2007; Kirby et al., 2006; Lee et al., 2009b), or (b) this part of the ECSZ experienced a strain transient as has been observed in the Mojave Desert (Rockwell et al., 2000; Peltzer et al., 2001; Oskin and Iriondo, 2004; Oskin et al., 2007). As described below, we propose that additional dextral slip on faults both to the west and east of the Fish Lake Valley and White Mountains fault zones may account for the apparent discrepancy, although dextral slip rates along many of these faults has not yet been determined.

To the west of the White Mountains fault zone, normal faults across the Volcanic Tableland extending into the southern part of Adobe Valley account for some of the discrepancy (Fig. 11). To our knowledge, Bateman (1965) was the first to suggest that the en echelon geometry of faults across the Tableland and axes of warping (adjacent broad anticlines and synclines) were the result of a “rotational couple” or dextral shear. Moreover, most of the \sim NS-striking normal faults strike clockwise with respect to Sierra Nevada-North America motion, thus defining releasing steps in a dextral shear zone (e.g. Unruh et al., 2003), and a few of these normal faults curve into parallelism with Sierra Nevada-North America motion suggesting that slip along these segments is dominantly dextral. Other investigators (e.g. Pinter, 1995; Phillips and Majkowski, 2001) have attributed the development of normal faults across the Volcanic Tableland to the

formation of an arch and flexure of the Bishop tuff. It is possible that faults exposed across the Volcanic Tableland developed as a consequence of both processes that acted broadly simultaneously. Further to the west, Phillips and Majkowski (2011) documented a component of dextral slip, in addition to normal slip, along the northern Round Valley fault, although a dextral slip rate was not determined. The dextral slip here projects northward into Long Valley caldera. There may be other faults throughout this region that also accommodate a component of NW-dextral shear.

To the east of the Fish Lake Valley fault zone, Frankel et al. (2007) suggested that dextral shear was accommodated via an extensional step-over through the Silver Peak-Lone Mountain extensional complex (Oldow et al., 1994; Hoesft and Frankel, 2010) and vertical axis rotation (Petronis et al., 2002; 2007).

Geodynamic Implications

Major fault slip across the Adobe Hills occurred after the eruption of a sequence of 3.43-3.13 Ma basalt flows. Early- to late Pliocene initiation of fault slip or renewed fault slip occurs throughout the western ECSZ-WLB-western Basin and Range between latitude $\sim 40^{\circ}\text{N}$ and 36°N including dextral slip across the northern WLB (Henry et al., 2007); extension across normal faults exposed along the eastern flank of the central Sierra Nevada (Henry & Perkins, 2001), the Tahoe-Truckee half graben (Surpluss et al., 2002), and the Wassuk Range front fault (Stockli et al., 2002); sinistral slip along the Coaldale fault located east of the Adobe Hills (Bradley, 2005; Lee et al., 2006); extension across the Queen Valley fault, and by fault slip transfer, dextral slip along the Owens Valley-White Mountains fault zone (Stockli et al., 2000, 2003); extension across the eastern Inyo fault zone (Lee et al., 2009a), Saline Range and Dry Mountains (Sternlof, 1988), and Malpais Mesa (Casteel, 2005); dextral slip along the Hunter Mountain fault (Lee et al., 2009a, Burchfiel et al., 1987; Sternlof, 1988); and transtension in the Coso geothermal field (Monastero et al., 2005). A change in plate boundary motion has not been documented for the Pliocene (Atwater and Stock, 1998), thus plate boundary forces do not appear to have been the trigger for the Pliocene age initiation of fault slip and renewal of fault slip within the western ECSZ-WLB-western margin of the Basin and Range Province. The trigger for this deformation episode may have been locally derived internal forces (gravitational potential energy) as a consequence of removal of lithosphere beneath the Sierra Nevada at ~ 3.5 Ma (e.g. Frassetto et al., 2011; Jones et al., 2004; Saleeby et al., 2003; Manly et al., 2000; Ducea and Saleeby, 1998; Ducea and Saleeby, 1996) if delamination extends northward beyond the southern Sierra Nevada (c.f. Zandt et al., 2004; Frassetto et al., 2011; Hammond et al., 2012).

CONCLUSIONS

New geologic mapping, structural, and $^{40}\text{Ar}/^{39}\text{Ar}$ geochronologic data from the Adobe Hills, western Mina deflection, highlight a history of pre-Pliocene deformation, rapid basalt flow emplacement during the late Pliocene, development of NNW-striking normal, NW-striking dextral, and NE-striking sinistral faults within a relatively short period of time, and a minimum late Pliocene sinistral slip rate of $\sim 0.4\text{-}0.5$ mm/yr. The dominance of NE-striking sinistral faults suggest that deformation across this part of the Mina deflection is characterized by a simple shear couple/fault block rotation, but paleomagnetic data are needed to test whether the blocks bounded by the sinistral faults rotated clockwise during fault slip. The sinistral faults in the Adobe Hills extend west of the predicted transfer of $0.8\text{-}0.4$ mm/yr Pliocene to Pleistocene dextral fault slip from the northern ECSZ into the western Mina deflection (Lee et al., 2009a).

We propose that a component of dextral slip along the Owens Valley fault is transferred into the Adobe Hills via dominantly normal, and to a lesser extent dextral, faults exposed across the Volcanic Tablelands, Benton Range, and southern Adobe Valley. The kinematics of fault slip transfer into the Adobe Hills occurs via a series of releasing bends in a zone dominated by dextral slip. This zone of dextral shear west of the White Mountains and Fish Lake Valley fault zones, along with other structures to the west and east of these fault zones, may account for the apparent discrepancy between summed long-term geologic dextral slip rates and geodetic strain rates across the northernmost part of ECSZ. The fault history we documented in the Adobe Hills is part of a regionally extensive early- to late-Pliocene onset or renewed deformation episode within the western Basin and Range. Deformation of this age stretches from the northern WLB ($\sim 40^\circ$) southward to the northern ECSZ ($\sim 36^\circ$) and is not associated with changes in plate motion, but coincides with the estimated timing of lithospheric drip from beneath the Sierra Nevada. This temporal and spatial relationship suggests that the Pliocene deformation episode was driven by locally derived internal forces.

Acknowledgements

Many thanks to Seth Pemble and Josh Stodola for their assistance and enthusiasm in the field, and to Chris Henry for discussions about the field relations in the Adobe Hills. This research was supported by a U.S. Geological Survey National Cooperative Geologic Mapping Program Award No. 08HQG0055 and a Central Washington University Seed Grant awarded to JL. SNR received additional funding from the University of California White Mountain Research Station Graduate Student Mini-grant Program, Central Washington University Graduate Studies and Research, and a Geological Society of America Graduate Student Research Grant. Thoughtful and constructive reviews from N. Niemi and anonymous resulted in an improved manuscript. The views and conclusions contained in this document are those of the authors and should not be interpreted as necessarily representing the official policies, either expressed or implied, of the U. S. Government.

REFERENCES

- Atwater, T. and Stock, J., 1998, Pacific-North America plate tectonics of the Neogene southwestern United States; an update: *International Geology Review*, v. 40, 375-402.
- Bateman, P. C., 1965, Geology and tungsten mineralization of the Bishop district, California: U. S. Geological Survey Professional Paper 470, 208 p.
- Bennett, R., Wernicke, B., Niemi, N. A., Friedrich, A. M., and Davis, J.L., 2003, Contemporary strain rates in the northern Basin and Range Province, United States: *Tectonics*, v. 22, 1008, doi: 10.1029/2001TC001355.
- Bradley, D., 2005, The Kinematic History of the Coaldale Fault, Walker Lane Belt, Nevada [M. S., Thesis]: Lawrence, Kansas, University of Kansas, 96 p.
- Burchfiel, B.C., and Stewart, J.H., 1966, "Pull-apart" origin of the central segment of Death Valley, California: *Geological Society of America Bulletin*, v. 77, p. 439-442, doi: 10.1130/0016-7606(1966)77[439:POOTCS]2.0.CO;2.
- Burchfiel, B.C., Hodges, K.V., and Royden, L.H., 1987, Geology of Panamint Valley-Saline Valley pull-apart system, California: Palinspastic evidence for low-angle geometry of a Neogene range-bounding fault: *Journal of Geophysical Research*, v. 92, p. 10,422-10,426, doi: 10.1029/JB092iB10p10422.

- Cashman, P. H., and Fontaine, S. A., 2000, Strain partitioning in the northern Walker Lane, western Nevada and northeastern California: *Tectonophysics*, v. 326, p. 111–130.
- Casteel, J.C., 2005, Late Miocene to Holocene faulting along the southwestern Inyo Mountains fault zone, eastern California [M.S. thesis]: Ellensburg, Washington, Central Washington University, 72 pp.
- Crowder, D.F. and Sheridan, M.F., 1972, Geologic map of the White Mountain peak quadrangle, Mono County, California: U.S. Geological Survey Map GQ-1012, scale 1:62,500.
- Cunningham, W.D., and Mann, P., eds., 2007, *Tectonics of Strike-Slip Restraining and Releasing Bends*: Geological Society of London Special Publication 290, 482 p.
- dePolo, C.M., Peppin, W.A., and Johnson, P.A., 1993, Contemporary tectonics, seismicity, and potential earthquake sources in the White Mountains seismic gap, west-central Nevada and east-central California, USA: *Tectonophysics*, v. 225, p. 271–299.
- Dilles, J., and Gans, P.B., 1995, The chronology of Cenozoic volcanism and deformation in the Yerington area, western Basin and Range and Walker Lane: *Geological Society of America Bulletin*, v. 107, p. 474–486, doi: 10.1130/0016-7606(1995)107<0474:TCOCVA>2.3.CO;2.
- Dixon T. H., Robaudo, S., Lee, J., and Reheis, M. C., 1995, Constraints on present-day Basin and Range deformation from space geodesy: *Tectonics*, v. 14, p. 755–772.
- Dixon, T. H., Miller, M., Farina, F., Wang, H., and Johnson, D., 2000, Present-day motion of the Sierra Nevada block and some tectonic implications for the Basin and Range province, North American Cordillera: *Tectonics*, v. 19, p. 1–24.
- Dokka, R. K., and Travis, C. J., 1990, Late Cenozoic strike-slip faulting in the Mojave Desert, California: *Tectonics*, v. 9, p. 311–340.
- Ducea, M.N., and Saleeby, J.B., 1996, Buoyancy sources for a large, unrooted mountain range, the Sierra Nevada, California: Evidence from xenoliths thermobarometry: *Journal of Geophysical Research*, v. 101, p. 8229–8244, doi: 10.1029/95JB03452.
- Ducea, M.N., and Saleeby, J.B., 1998, A case for delamination of the deep batholithic crust beneath the Sierra Nevada, California: *International Geology Review*, v. 40, p. 78–93, doi: 10.1080/00206819809465199.
- Frankel, K. L., Dolan, J. F., Finkel, R. C., Owen, L. A., and Hoeft, J. S., 2007, Spatial variations in slip rate along the Death Valley-Fish Lake Valley fault system determined from LiDAR topographic data and cosmogenic ¹⁰Be geochronology: *Geophysical Research Letters*, v. 34, p. 1–6.
- Frassetto, A.M., Zandt, G., Gilbert, H., Owens, T.J., and Jones, C.H., 2011, Structure of the Sierra Nevada from receiver functions and implications for lithospheric foundering: *Geosphere*, v. 7, p. 898–921, doi: 10.1130/GES00570.1.
- Gilbert, C.M., Christensen, M N., Yehya Al-Rawl, and Lajoie, K.R., 1968, *Structural and Volcanic History of Mono Basin, California-Nevada: A memoir in honor of Howel Williams*: Geological Society of America Memoir, v. 116, p.275–329.
- Hammond, W.C., Blewitt, G., Li, Zhenhong, Plag, H.-P., and Kreemer, C., 2012, Contemporary uplift of the Sierra Nevada, western United States, from GPS and InSAR measurements: *Geology*, doi: 10.1130/G32968.1.
- Henry, C.D., Faulds, J.E., and dePolo, C.M., 2007, Geometry and timing of strike-slip and normal faults in the northern Walker Lane, northwestern Nevada and northeastern California: Strain partitioning or sequential extensional and strike-slip deformation?, *in* Till, A.B., Roeske, S.M., Sample, J.C., and Foster, D.A., eds., *Exhumation Associated with Continental*

- Strike-Slip Fault Systems: Geological Society of America Special Paper 434, p. 59–79, doi: 10.1130/2007.2434(04).
- Henry, C.D. and Perkins, M.E., 2001, Sierra Nevada-Basin and Range transition near Reno, Nevada: Two-stage development at 12 and 13 Ma: *Geology*, v. 29, p. 719-722.
- Jones, C.H., Farmer, G.L., and Unruh, J., 2004, Tectonics of Pliocene removal of lithosphere of the Sierra Nevada, California: *Geological Society of America Bulletin*, v. 116, 1408-1422.
- Kirby, E., Anandkrishnan, S., Phillips, F., and Marrero, S., 2008, Late Pleistocene slip rate along the Owens Valley fault, eastern California: *Geophysical Research Letters*, v. 35, L01304, doi:10.1029/2007GL031970.
- Kirby, E., Burbank, D., Reheis, M., and Phillips, F., 2006, Temporal variations in slip rate of the White Mountain Fault Zone, Eastern California: *Earth and Planetary Science Letters*, v. 248, p. 153–170.
- Krauskopf, K.B. and Bateman, P.C., 1977, Geologic map of the Glass Mountain Quadrangle, Mono County, California, and Mineral County, Nevada: U.S. Geological Survey Geologic Quadrangle Map GQ-1099, scale 1:62,500.
- Lee, J., Stockli, D. F., Owen, L. A., Finkel, R. C., and Kislitsyn, R., 2009a, Exhumation of the Inyo Mountains, California: Implications for the timing of extension along the western boundary of the Basin and Range Province and distribution of dextral slip rates across the eastern California shear zone: *Tectonics*, v. 28, 20 p., doi: 10.1029/2008TC002295.
- Lee, J., Garwood, J., Stockli, D., and Gosse, J., 2009b, Quaternary faulting in Queen Valley, California-Nevada: Implications for kinematics of fault slip transfer in the Eastern California Shear Zone-Walker Lane Belt: *Geological Society of America Bulletin*, v. 121, p. 599–614, doi: 10.1130/B26352.1.
- Lee, J., Rubin, C. M., and Calvert, A., 2001, Quaternary faulting history along the Deep Springs fault, California: *Geological Society of America Bulletin*, v. 113, p. 855-869.
- Lee, J., Stockli, D., Schroeder, J., Tincher, C., Bradley, D., Owen, L., Gosse, J., Finkel, R., and Garwood, J., 2006, Fault slip transfer in the Eastern California Shear Zone-Walker Lane Belt: *Geological Society of America Penrose Conference Field Trip Guide (Kinematics and Geodynamics of Intraplate Dextral Shear in Eastern California and Western Nevada, Mammoth Lakes, California, 21-26 April 2005)*, 26 p., doi: 10.1130/2006.FSTITE.PFG.
- Manley, C.R., Glazner, A.F., and Farmer, G.L., 2000, Timing of volcanism in the Sierra Nevada of California: Evidence for Pliocene delamination of the batholithic root?: *Geology*, v. 28, p. 811–814.
- McClay, K., and Dooley, T., 1995, Analogue models of pull apart basins: *Geology*, v. 23, p. 711–714, doi: 10.1130/0091-7613(1995)023<0711:AMOPAB>2.3.CO;2.
- McKenzie, D., and Jackson, J., 1983, The relationship between strain rates, crustal thickening, paleomagnetism, finite strain and fault movements within a deforming zone: *Earth and Planetary Science Letters*, v. 65, p. 182–202.
- McKenzie, D., and Jackson, J., 1986, A block model of distributed deformation by faulting: *Journal of the Geological Society of London*, v. 143, p. 349–353.
- Monastero, F.C., Katzenstein, A.M., Miller, J.S., Unruh, J.R., Adams, M.C., and Richards-Dinger, 2005, The Coso geothermal field: A nascent metamorphic core complex: *Geological Society of America Bulletin*, v. 117, p. 1534-1553; doi: 10.1130/B25600.1.
- Nevin, A.E., 1963, Late Cenozoic stratigraphy and structure of the Benton area, Mono County, California [M.A. thesis]: Berkeley, California, University of California, Berkeley, 62 p.

- Oldow, J.S., 1992, Late Cenozoic displacement partitioning in the northwestern Great Basin, *in* Lane, C., and Steven, D., eds., Geological Society of Nevada Walker Lane Symposium: Structure, Tectonics and Mineralization of the Walker Lane: Reno, Geological Society of Nevada, p. 17–52.
- Oldow, J.S., 2003, Active transtensional boundary zone between the western Great Basin and Sierra Nevada block, western U.S. Cordillera: *Geology*, v. 31, p. 1033–1036, doi: 10.1130/G19838.1.
- Oldow, J.S., Bally, A.W., Lallemand, H.G.A., and Leeman, W.P., 1989, Phanerozoic evolution of the North American Cordillera; United States and Canada, *in* Bally, A.W., and Palmer, A.R., eds., *An Overview: Boulder, Colorado*, Geological Society of America, *Geology of North America*, v. A, p. 139–232.
- Oldow, J. S., Kohler, G., and Donelick, R. A., 1994, Late Cenozoic extensional transfer in the Walker Lane strike-slip belt, Nevada: *Geology*, v. 22, p. 637–640.
- Oldow, J.S., Elias, E.A., Ferranti, L., McClelland, W.C., and McIntosh, W.C., 2009, Late Miocene to Pliocene synextensional deposition in fault-bounded basins within the upper plate of the western Silver Peak–Lone Mountain extensional complex, west-central Nevada: *in* Oldow, J.S. and Cashman, P.H., *Late Cenozoic structure and evolution of the Great Basin–Sierra Nevada transition*, Geological Society of America Special Paper, v. 447, pp. 275–312.
- Onstott, T.C., Miller, M.L., Ewing, R.C., and Walsh, D., 1995, Recoil refinements: Implications for the $^{40}\text{Ar}/^{39}\text{Ar}$ dating technique: *Geochim. Cosmochim. Acta* 59, 1821–1834.
- Oskin, M., Perg, L., Blumentritt, D., Mukhopadhyay, S., and Iriondo, A., 2007, Slip rate of the Calico fault: Implications for geologic versus geodetic rate discrepancy in the Eastern California Shear Zone: *Journal of Geophysical Research-Solid Earth*, v. 112, 10.1029/2006JB004451.
- Oskin, M. and Iriondo, A., 2004, Large-magnitude transient strain accumulation on the Blackwater fault, Eastern California shear zone: *Geology*, v. 32, 313–316.
- Oswald, J.A., and Wesnousky, S.G., 2002, Neotectonics and Quaternary geology of the Hunter Mountain fault zone and Saline Valley region, southeastern California: *Geomorphology*, v. 42, p. 255–278, doi: 10.1016/S0169-555X(01)00089-7.
- Peltzer, G., Crampe, F., Hensley, S., and Rosen, P., 2001, Transient strain accumulation and fault interaction in the Eastern California shear zone, *Geology*, v. 29, 975–978.
- Petronis, M.S., Geissman, J.W., Oldow, J.S., and McIntosh, W.C., 2009, Late Miocene to Pliocene vertical-axis rotation attending development of the Silver Peak–Lone Mountain displacement transfer zone, west-central Nevada: Geological Society of America Special Paper, v. 447, p. 215–253, doi: 10.1130/2009.2447(12).
- Petronis, M.S., Geissman, J.W., Oldow, J.S., and McIntosh, W.C., 2007, Tectonism of the southern Silver Peak Range: Paleomagnetic and geochronologic data bearing on the Neogene development of a regional extensional complex, central Walker Lane, Nevada: Geological Society of America Special Paper 434, 106 p.
- Phillips, F.M. and Majkowsi, L., 2011, The role of low-angle normal faulting in active tectonics of the northern Owens Valley California: *Lithosphere*, v. 3, p. 22–36, doi: 10.1130/L73.1.
- Pinter, N., 1995, Faulting on the Volcanic Tableland, Owens Valley, California: *The Journal of Geology*, v. 103, p. 73–83.

- Reheis, M.C., Stine, S., and Sarna-Wojcicki, A.M., 2002, Drainage reversals in Mono Basin during the late Pliocene and Pleistocene: *Geological Society of America Bulletin*, v. 114, p. 991–1006.
- Reheis, M.C., and Dixon, T.H., 1996, Kinematics of the Eastern California shear zone: Evidence for slip transfer from Owens and Saline Valley fault zones to Fish Lake Valley fault zone: *Geology*, v. 24, p. 339–342.
- Rinehart, C.D. and Ross, D.C., 1957, Geologic map of Casa Diablo Mountain Quadrangle, California: U.S. Geological Survey Geologic Quadrangle Map GQ-99, scale 1:62,500.
- Rockwell, T.K., Lindvall, S., Herzberg, M., Murbach, D., Dawson, T., and Berger, G., 2000, Paleoseismology of the Johnson Valley, Kickapoo, and Homestead Valley faults: Clustering of earthquakes in the eastern California shear zone: *Bulletin of the Seismological Society of America*, v. 90, 1200–1236.
- Rogers, A.M., Harmsen, S.C., Corbett, E.J., Priestly, K., and dePolo, D., 1991, The seismicity of Nevada and some adjacent parts of the Great Basin, *in* Slemmons, D.B., et al., eds., *Neotectonics of North America: Boulder, Colorado, Geological Society of America, Decade Map Volume 1*, p. 153–184.
- Rood, D.H., Burbank, D.W., Herman, S.W., and Bogue, S., 2011, Rates and timing of vertical-axis block rotations across the central Sierra Nevada-Walker Lane transition in the Bodie Hills, California/Nevada: *Tectonics*, v. 30, TC5013, doi:10.1029/2010TC002754.
- Ryall, A.S., and Priestly, K., 1975, Seismicity, secular strain, and maximum magnitude in the Excelsior Mountains area, western Nevada and eastern California: *Geological Society of America Bulletin*, v. 86, p. 1585–1592.
- Saleeby, J., Ducea, M., and Clemens-Knott, D., 2003, Production and loss of high-density batholithic root, southern Sierra Nevada, California: *Tectonics*, v. 22, doi: 10.1029/2002TC001374.
- Sarna-Wojcicki, A., Pringle, M.S., and Wijbrans, J., 2000, New $^{40}\text{Ar}/^{39}\text{Ar}$ age of the Bishop tuff from multiple sites and sediment rate calibration for the Matuyama-Brunhes boundary: *Journal of Geophysical Research—Solid Earth*, v. 105, p. 21,431–21,443.
- Sheehan, T.P., 2007, Evolution of Neogene fault populations in northern Owens Valley, California and implications for the Eastern California shear zone [Ph.D. thesis]: New Orleans, Louisiana, Tulane University, 203 p.
- Sternlof, K.R., 1988, Structural style and kinematic history of the active Panamint-Saline extensional system, Inyo County, California [M.S. thesis]: Cambridge, Massachusetts, Massachusetts Institute of Technology, 40 p.
- Stockli, D.F., Surpless, B.E., Dumitru, T.A., and Farley, K.A., 2002, Thermochronological constraints on the timing and magnitude of Miocene and Pliocene extension in the central Wassuk Range, western Nevada, *Tectonics*, v. 21, 10.1029/2001TC001295.
- Stockli, D.F., Farley, K.A., and Dumitru, T.A., 2000, Calibration of the apatite (U-Th)/He thermochronometer on an exhumed fault block, White Mountains, California: *Geology*, v. 28, p. 983–986, doi: 10.1130/0091-7613(2000)28<983:COTAHT>2.0.CO;2.
- Stockli, D.F., Dumitru, T.A., McWilliams, M.O., and Farley, K.A., 2003, Cenozoic tectonic evolution of the White Mountains, California and Nevada: *Geological Society of America Bulletin*, v. 115, 788–816.

- Surpless, B.E., Stockli, D.F., Dumitru, T.A., and Miller, E.L., 2002, Two-phase westward encroachment of Basin and Range extension into the northern Sierra Nevada: *Tectonics*, v. 21, 10.1029/2000TC001257.
- Tincher, C.R. and Stockli, D.F., 2009, Cenozoic volcanism and tectonics in the Queen Valley area, Esmeralda County, western Nevada, in Oldow, J.S. and Cashman, P.H., Late Cenozoic structure and evolution of the Great Basin-Sierra Nevada transition, *Geological Society of America Special Paper*, v. 447, pp. 255-274.
- Tosdal, R.M., Wooden, J.L., and Kistler, R.W., 2000, Geometry of the Neoproterozoic continental break-up, and implications for location of Nevadan mineral belts, *in* Cluer, J.K., Price, J.G., Struhsacker, E.M., Hardyman, R.F., and Morris, C.L., eds., *Geology and Ore Deposits 2000: The Great Basin and Beyond: Geological Society of Nevada Symposium Proceedings*, May 15-18, 2000, p. 451-466.
- Turner, G. and Cadogan, P.H., 1974, Possible effects of ^{39}Ar recoil in ^{40}Ar - ^{39}Ar dating: *Geochim. Cosmochim. Acta* 5, Supplement, 1601-1615.
- Unruh, J., Humphrey, J., and Barron, A., 2003, Transtensional model for the Sierra Nevada frontal fault system, eastern California: *Geology*, v. 31, p. 327-330.
- Wesnousky, S.G., 2005, Active faulting in the Walker Lane: *Tectonics*, v. 24, TC3009, p. 1-35.
- Zandt, G., Gilbert, H., Owens, T.J., Ducea, M., Saleeby, J., and Jones, C.H., 2004, Active foundering of a continental arc root beneath the southern Sierra Nevada in California: *Nature*, v. 431, p. 41-46, doi: 10.1038/nature02847.

FIGURE CAPTIONS

Figure 1. A. Simplified tectonic map of the western U.S. Cordillera showing the modern plate boundaries and tectonic provinces. Basin and Range Province is in medium gray; CNSB (Central Nevada seismic belt), ECSZ (eastern California shear zone), ISB (Intermountain seismic belt), and WLB (Walker Lane belt) are in light gray; MD (Mina deflection) is in dark gray. B. Shaded relief map of the Walker Lane Belt and northern part of the eastern California shear zone showing the major Quaternary faults. Solid ball is located on the hanging wall of normal faults; arrow pairs indicate relative motion across strike-slip faults; white dashed box outlines location of Figure 2; light gray shaded areas show the Mina deflection and the Carson domain. Fault abbreviations: BSF—Benton Springs fault; CF—Coaldale fault; DSF—Deep Springs fault; DVFCFLVFZ—Death Valley–Furnace Creek–Fish Lake Valley fault zone; GHF—Gumdrop Hills fault; HLF—Honey Lake fault; HMF—Hunter Mountain fault; MVF—Mohawk Valley fault; OVF—Owens Valley fault; PLF—Pyramid Lake fault; PSF—Petritified Springs fault; QVF Queen Valley fault; SLF—Stateline fault; SNFFZ—Sierra Nevada frontal fault zone; WMFZ—White Mountains fault zone; WRF—Wassuk Range fault; WSFZ—Warm Springs fault zone.

Figure 2. Shaded relief map of the southern part of the Mina deflection and northern part of the eastern California shear zone showing the major Quaternary faults. Solid black ball is located on the hanging wall of normal faults; arrow pairs indicate relative motion across strike-slip faults. Heavy arrow in northwest corner of map shows the present day motion of the Sierra Nevada with respect to North America (Dixon et al., 2000). Location of the Adobe Hills geologic map shown in Figure 5 is outlined with a dashed line and location of this map is shown in Figure 1. Fault abbreviations: CF—Coaldale fault; CSF, Coyote Springs fault; DSF, Deep Springs fault;

FLVFZ—Fish Lake Valley fault zone; HCF, Hilton Creek fault; OVF, Owens Valley fault; QVF—Queen Valley fault; RVF, Round Valley fault; WMFZ—White Mountains fault zone.

Figure 3. Block diagrams illustrating models proposed to explain fault slip transfer across the Mina deflection. (A) Displacement-transfer model in which normal slip along connecting faults transfers fault slip (modified from Oldow, 1992; Oldow et al., 1994). (B) Transtensional model showing a combination of sinistral and normal slip along connecting faults. (C) Clockwise block rotation model in which sinistral slip along connecting faults, combined with vertical axis rotation of intervening fault blocks, transfer fault slip (modified from McKenzie and Jackson, 1983, 1986). Single-barbed arrows show dextral fault motion across faults of the ECSZ and WLB and sinistral motion along faults in the Mina deflection; half-circle double-barbed arrows indicate clockwise rotating fault blocks; solid ball is located on the hanging wall of normal slip faults; thin short lines indicate slip direction on fault surfaces.

Figure 4. Geologic map of the Adobe Hills region (1:24,000 scale). See Figure 2 for location.

Figure 5. Interpretative NW-SE and EW cross-sections. Note that vertical scale is two times the horizontal scale for cross-section AA', that the two cross-sections are not at the same scale, and that both cross-sections are at a smaller scale than the geologic map shown in Figure 4. See Figure 4 for location of sections.

Figure 6. Stratigraphic column of Miocene and Pliocene volcanic and sedimentary rocks exposed in the Adobe Hills. Relative thicknesses are shown.

Figure 7. Age spectra for plagioclase within ignimbrite and groundmass concentrate within basalt flows. Summary of ages is shown in Table 1 and analytical data are listed in Data Repository #.

Figure 8. Fault map of the Adobe Hills compiled on digital orthophotographs highlighting primary sinistral fault zones and location of measured lateral offset. Normal faults shown in white; sinistral and dextral faults shown in black. Solid ball, hachures, and paired arrows are defined in Figure 2. See text for discussion of slip calculations along transects.

Figure 9. Field photograph of a playa formed in an extensional step-over or releasing bend along a left-stepping sinistral fault. Paired arrows show relative strike-slip fault motion; solid ball is on the hanging wall of the normal fault. Abbreviations are: Q, undifferentiated Quaternary sediments; Qp, Quaternary playa deposits; and Pb, undifferentiated Pliocene basalts.

Figure 10. Detailed fault maps superimposed on digital orthophotographs and DEM generated contours showing left lateral offset of geologic features along sinistral faults 2 and 3 (see Figure 8). (A) The intersection line of a normal fault and the surface of its hanging wall basin are sinistrally offset twice for a total of ~695 m along the northeastern segment of fault 2. (B) The southwestern segment of fault 2 is characterized by several subparallel sinistral fault strands that offset the intersection of line of normal faults and hanging wall basins, and a basalt ridgeline (narrow dashed line). The net offset across these sinistral faults is ~523 m. (C) The edge of the

basalt rubble flow, unit Pbr, is sinistrally offset ~527 m by fault 3. Paired arrows, solid ball, and hachures are defined in Figure 4, and figure locations are shown in Figure 4.

Figure 11. Simplified map highlighting the kinematic link between the Owens Valley fault and sinistral faults in the Adobe Hills. Map shows faults from the Bishop region northward to the Adobe Hills where each major fault or fault zone is shown as a single fault (compare to fault maps in Figs. 2 and 8). Large arrow indicates motion of the Sierra Nevada microplate (SN) with respect to a fixed North American plate (NA) (Dixon et al., 2000). Colored arrows with adjacent numbers indicate fault slip vectors and slip rate in mm/yr. Red arrows show the calculated 0.6 mm/yr ENE-WSW extension across the southern part of Adobe Valley (Benton Range and Black Mountain). Blue arrows and adjacent slip rates indicate the partitioning of the 0.6 mm/yr vector into parallel and perpendicular vectors along NW-striking oblique-slip faults in the eastern Adobe Valley and NE-striking sinistral faults in the Adobe Hills. See text for discussion. Solid ball is on the hanging wall of normal faults and paired arrows indicate relative motion across strike-slip faults. Fault abbreviations: CF—Coaldale fault; CSF, Coyote Springs fault; OVF, Owens Valley fault; QVF—Queen Valley fault; WMFZ—White Mountains fault zone.

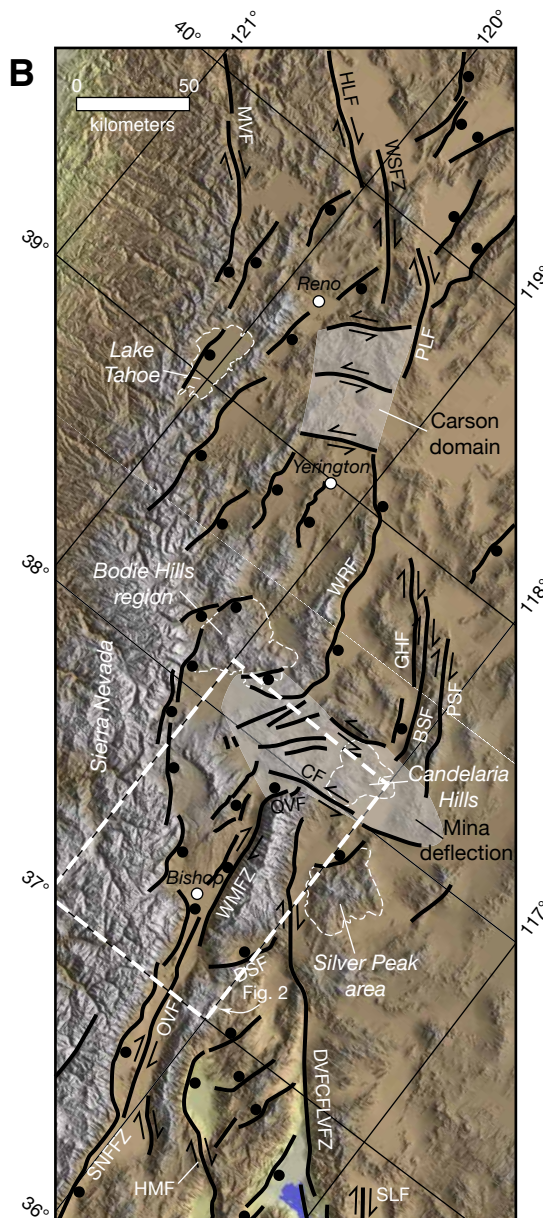
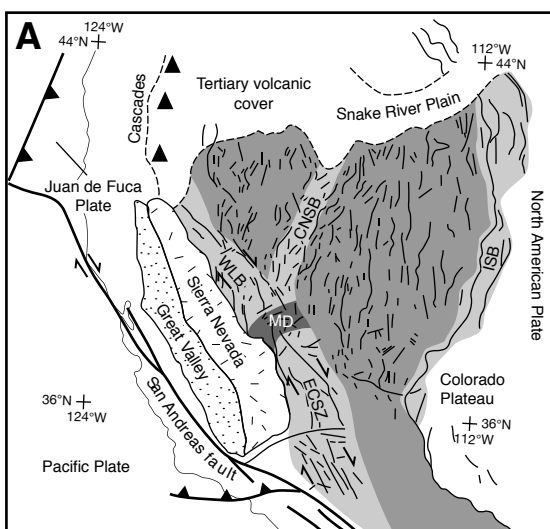


Figure 1. A. Simplified tectonic map of the western U.S. Cordillera showing the modern plate boundaries and tectonic provinces. Basin and Range Province is in medium gray; CNSB (Central Nevada seismic belt), ECSZ (eastern California shear zone), ISB (Intermountain seismic belt), and WLB (Walker Lane belt) are in light gray; MD (Mina deflection) is in dark gray. **B.** Shaded relief map of the Walker Lane Belt and northern part of the eastern California shear zone showing the major Quaternary faults. Solid ball is located on the hanging wall of normal faults; arrow pairs indicate relative motion across strike-slip faults; white dashed box outlines location of Figure 2; light gray shaded areas outline the Mina deflection and Carson domain. Fault abbreviations: BSF—Benton Springs fault; CF—Coaldale fault; DSF—Deep Springs fault; DVFCFLVFZ—Death Valley–Furnace Creek–Fish Lake Valley fault zone; GHF—Gumdrop Hills fault; HLF—Honey Lake fault; HMF—Hunter Mountain fault; MVF—Mohawk Valley fault; OVF—Owens Valley fault; PLF—Pyramid Lake fault; PSF—Petrified Springs fault; QVF—Queen Valley fault; SLF—Stateline fault; SNFFZ—Sierra Nevada frontal fault zone; WMFZ—White Mountains fault zone; WRF—Wassuk Range fault; WSFZ—Warm Springs fault zone.

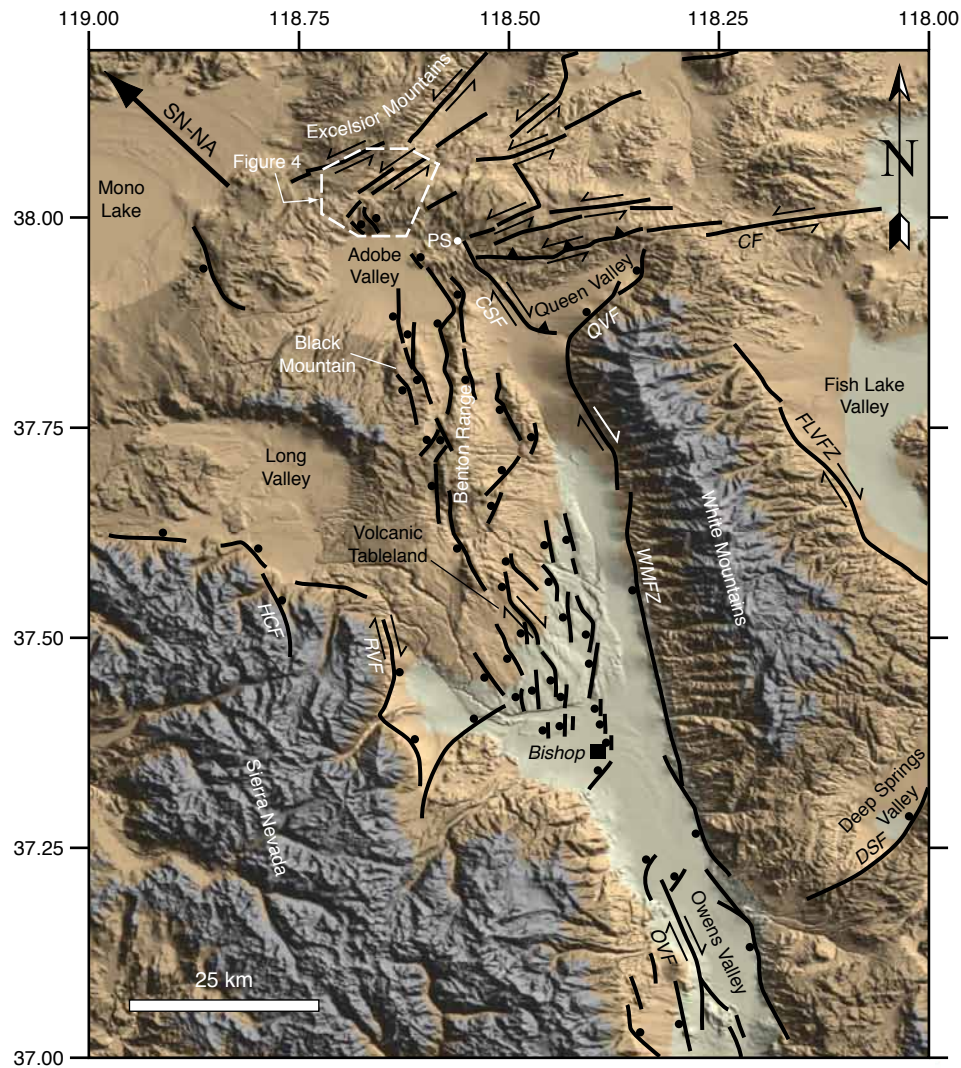


Figure 2. Shaded relief map of the southern part of the Mina deflection and northern part of the eastern California shear zone showing the major Quaternary faults. Solid black ball is located on the hanging wall of normal faults; arrow pairs indicate relative motion across strike-slip faults; PS indicates location of Pizona Springs. Heavy arrow in northwest corner of map shows the present day azimuth of Sierra Nevada motion with respect to North America (Dixon et al., 2000). Location of the Adobe Hills geologic map shown in Figure 4 is outlined with a dashed line and location of this map is shown in Figure 1. Fault abbreviations: CF—Coaldale fault; CSF, Coyote Springs fault; DSF, Deep Springs fault; FLVFZ—Fish Lake Valley fault zone; HCF, Hilton Creek fault; OVF, Owens Valley fault; QVF—Queen Valley fault; RVF, Round Valley fault; WMFZ—White Mountains fault zone.

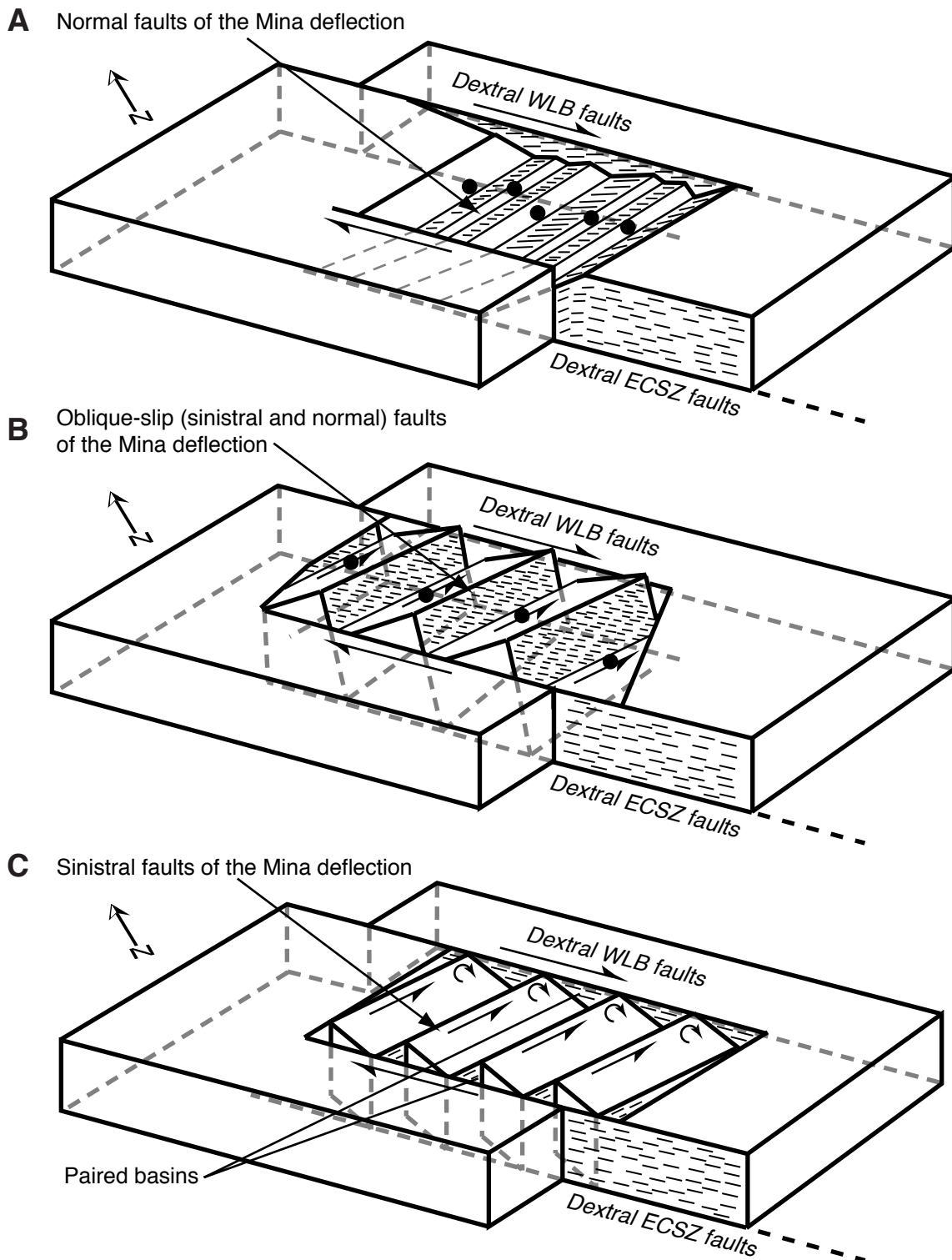
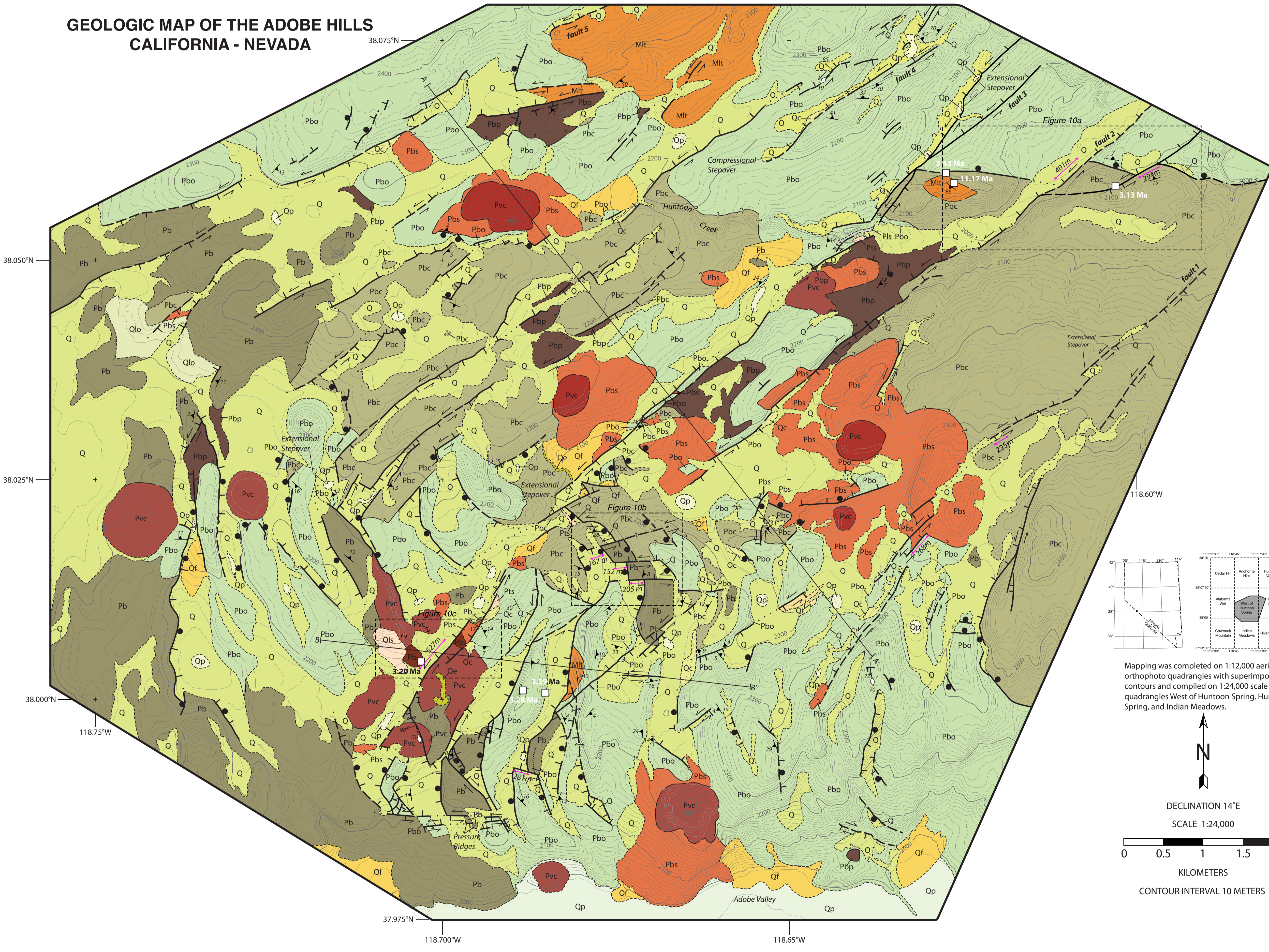


Figure 3. Block diagrams illustrating models proposed to explain fault slip transfer across the Mina deflection. (A) Displacement-transfer model in which normal slip along connecting faults transfers fault slip (modified from Oldow, 1992; Oldow et al., 1994). (B) Transtensional model showing a combination of sinistral and normal slip along connecting faults. (C) Clockwise block rotation model in which sinistral slip along connecting faults, combined with vertical axis rotation of intervening fault blocks, transfer fault slip (modified from MacKenzie and Jackson, 1983, 1986; Wesnousky, 2005). Single-barbed arrows show dextral fault motion across faults of the ECSZ and WLB and sinistral motion along faults in the Mina deflection; half-circle double-barbed arrows indicate clockwise rotating fault blocks; solid ball is located on the hanging wall of normal slip faults; thin short lines indicate slip direction on fault surfaces.

**GEOLOGIC MAP OF THE ADOBE HILLS
CALIFORNIA - NEVADA**

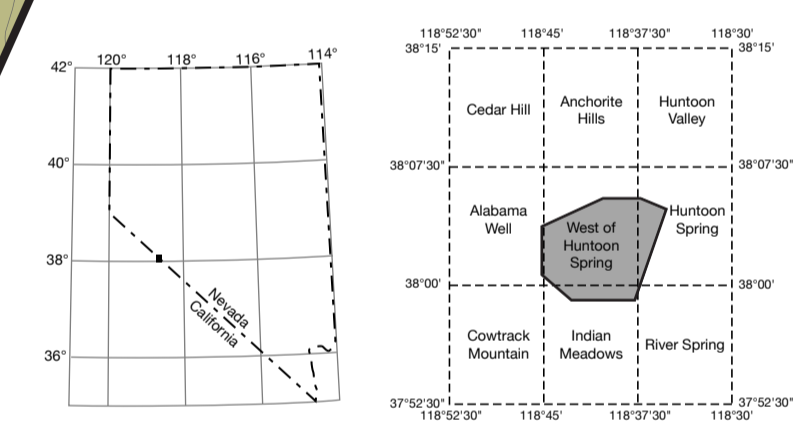


EXPLANATION

- Sedimentary and Volcanic Units**
- Qc** **Aeolian tuffaceous sand.** White sand containing tabular pumice fragments up to ~8 mm, glass shards, and quartz grains.
 - Q** **Undifferentiated sediments.** Aeolian tuffaceous sand, fan deposits, and playa deposits following Reheis et al. (2002).
 - Qp** **Terrace.** Fluvial sediments deposited upon basalt bedrock proximal to a channel.
 - Qf** **Playa deposits.** White silt to mud-sized shallow-water playa deposits.
 - Qls** **Fan deposits.** Angular basalt cobbles to boulders and aeolian tuffaceous sand that define a convex up, fan morphology.
 - Qc** **Landslide deposits.** Angular basalt cobbles to boulders that define a hummocky surface.
 - Qc** **Basalt colluvium.** Angular basalt cobbles to boulders sourced up slope; common near fault scarps.
 - Qlo** **Beach gravel.** White, chalky, massive carbonate deposits mantling basalts in the western Adobe Hills. Gravel-sized clasts and gastropod fossils are common. This unit is interpreted to represent middle to early Pleistocene high stands of Mono Lake (Reheis et al., 2002).
 - Pbs** **Basalt scoria.** Red and black scoria deposits ranging in size from near sand to cobble with scarce phenocrysts of olivine, pyroxene, and plagioclase. Sourced from nearby volcanic center.
 - Pvc** **Volcanic center.** Red weathering, commonly cone-shaped volcanic center with smaller than pebble sized basalt cinder, pebble to cobble-sized scoria, and volcanic bombs and blocks, and vesicular breccia blocks.
 - Pbp** **Basalt lava.** Brown to tan weathering, light to medium gray, weakly phytic (~1%) basalt lava. Phenocrysts consist of euhedral, translucent plagioclase within a crystalline groundmass. **Pbo**—Brown weathering, light to dark gray, flaggy, weakly phytic (<1%) basalt lava. Phenocrysts consist of euhedral to subhedral olivine (1-2 mm) and pyroxene (1-2 mm) in a microcrystalline groundmass. ⁴⁰Ar/³⁹Ar geochronology on basalt groundmass records ages of 3.28 ± 0.03 Ma and 3.39 ± 0.03 Ma. **Pb**—Basalt lava rubble characterized by rounded cobble to boulder-sized clasts of black, vesicular, phytic basalt. Phenocrysts include zoned pyroxene, olivine, and plagioclase in a coarse crystalline groundmass. ⁴⁰Ar/³⁹Ar geochronology on basalt groundmass yields an age of 3.20 ± 0.03 Ma. **Pbc**—Red to brown weathering, light to dark gray, phytic basalt lava. Phenocrysts consist of 5-10% glomerocrysts of euhedral to subhedral pyroxene (1-7 mm) and olivine (1-4 mm), and trace plagioclase phenocrysts (<1 mm) in a crystalline groundmass. ⁴⁰Ar/³⁹Ar geochronology on basalt groundmass yields ages of 3.13 ± 0.02 Ma and 3.43 ± 0.01 Ma. **Pb**—Undifferentiated basalt lava.
 - Pts** **Tuffaceous sandstone.** Tan to light orange weathering, tan to brown, fine- to medium-grained, poorly sorted, moderately friable, tuffaceous sandstone comprised of 10% angular to subangular tabular pumice clasts (1-4 mm), 3% angular and subrounded obsidian, and scoria lithics (1-2 mm).
 - Pli** **Lacustrine sediments.** Alternating beds of tan cross-bedded sandstones and white, silt-sized siliceous lake deposits underlying basalt lavas.
 - Mit** **Latite ignimbrite.** Unwelded to welded, biotite-bearing latite ignimbrite deposits variable in color. The unwelded ignimbrite underlies basalts in the southern Adobe Hills and is dark brown to ashy black, friable, and contains 4% subrounded basalt (4-5 mm), subangular red granite (~3 mm), and wood lithics. Minerals include 0.5% euhedral biotite (<1 mm) and 0.5% subhedral plagioclase (1-2 mm). Visible flow features are absent. The welded ignimbrite, which is a ridge-former mantled by younger basalt lavas in the northern Adobe Hills, is white, pink, or dark gray in color, porphyritic, with gray to dark gray angular basalt lithics up to 30 mm in diameter. Phenocrysts include ~1% euhedral-subhedral biotite (1-2 mm) and ~1% gray to clear plagioclase (1-2 mm) within an aphanitic groundmass. Some flows exhibit eutaxitic texture. ⁴⁰Ar/³⁹Ar geochronology on plagioclase yields an age of 11.17 ± 0.04 Ma for this unit.

SYMBOLS

- Contacts**
- Solid where well-located (≤10m), dashed where approximately located (≤20m), dotted where concealed, queried where speculative.
 - Arrow indicates contact dip direction and magnitude.
 - Unit Q contact.
- Faults**
- Normal fault, ball and hachures on hanging wall; solid where well located (≤10m), dashed where approximately located (≤20m), dotted where concealed. Double-pronged arrow indicates fault plane dip direction and magnitude; diamond-headed arrow shows trend and plunge of fault striation.
 - Strike slip fault, paired arrows indicate relative sense of lateral slip, hachures on relative downthrown side; solid where well located (≤10m), dashed where approximately located (≤20m), dotted where concealed.
 - 527m magnitude of lateral offset
- Intrusive rocks**
- dike
- Attitudes**
- bedding
 - flow foliation
- Geochronology**
- ⁴⁰Ar/³⁹Ar sample location and age in Ma



Mapping was completed on 1:12,000 aerial digital orthophoto quadrangles with superimposed contours and compiled on 1:24,000 scale USGS quadrangles West of Hutton Spring, Hutton Spring, and Indian Meadows.

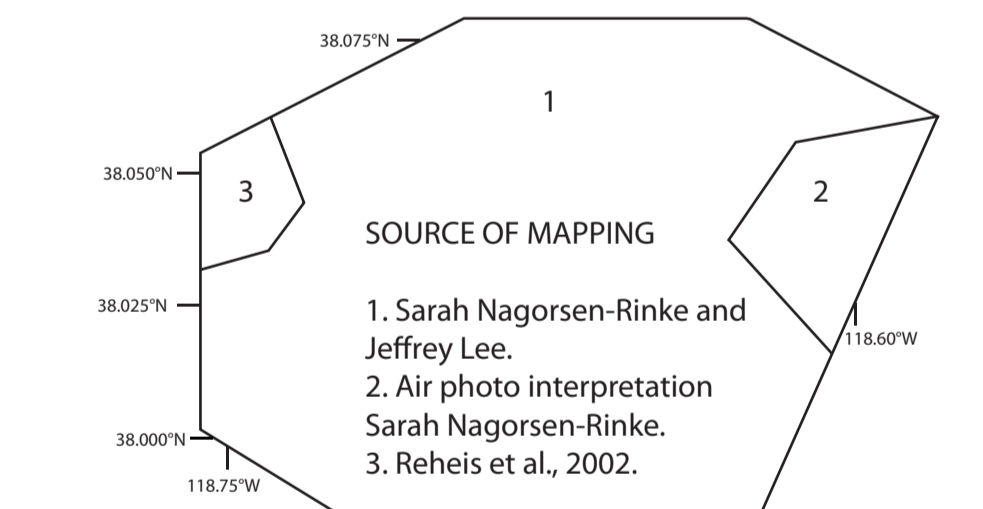
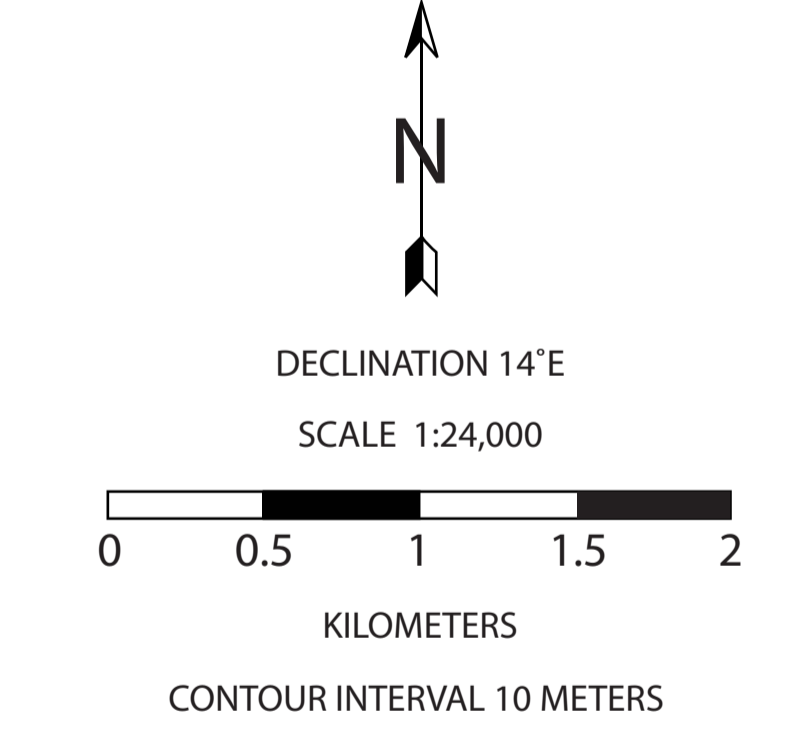


Figure 4. Geologic map of the Adobe Hills region (1:24,000 scale). Location shown in Figure 2.

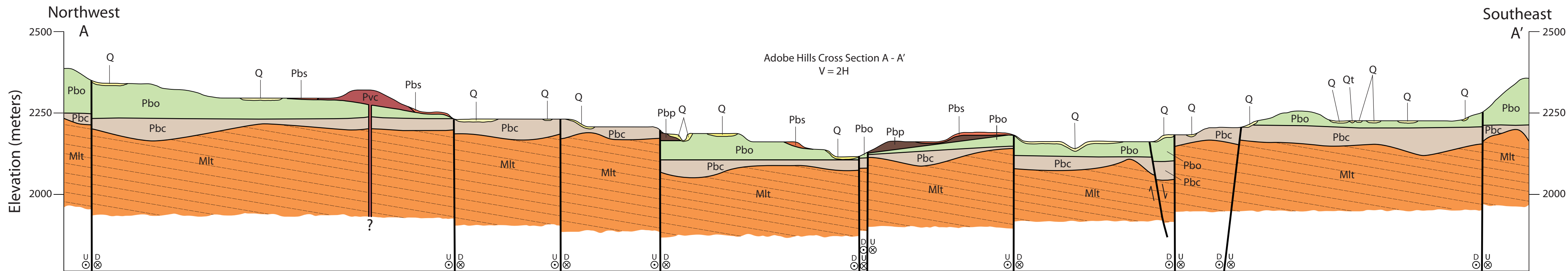


Figure 5. Interpretative NW-SE and EW cross-sections. Note that vertical scale is two times the horizontal scale for cross-section AA', that the two cross-sections are not at the same scale, and that both cross-sections are at a smaller scale than the geologic map shown in Figure 4. See Figure 4 for location of sections.

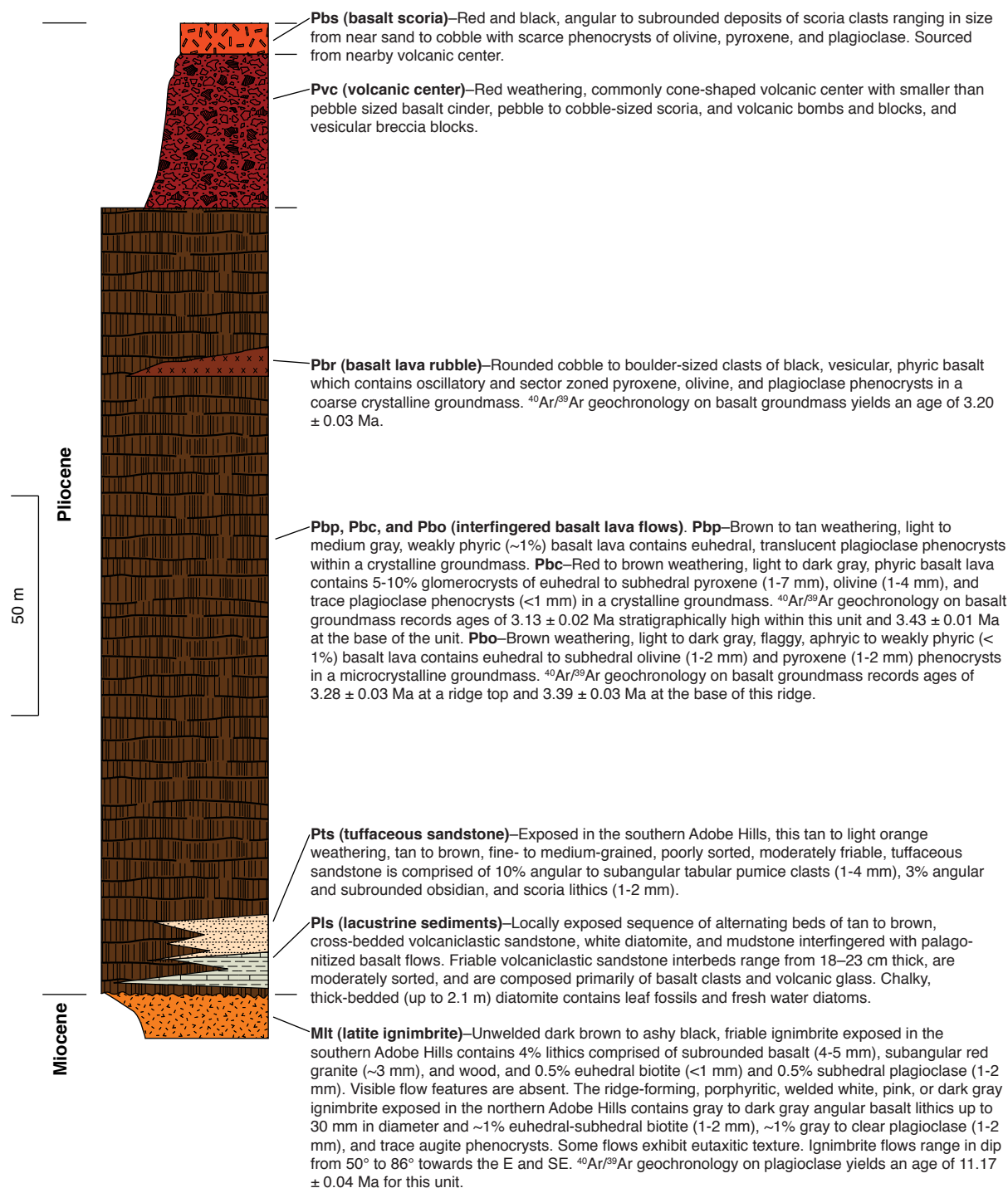


Figure 6. Stratigraphic column of Miocene and Pliocene volcanic and sedimentary rocks exposed in the Adobe Hills. Relative thicknesses are shown.

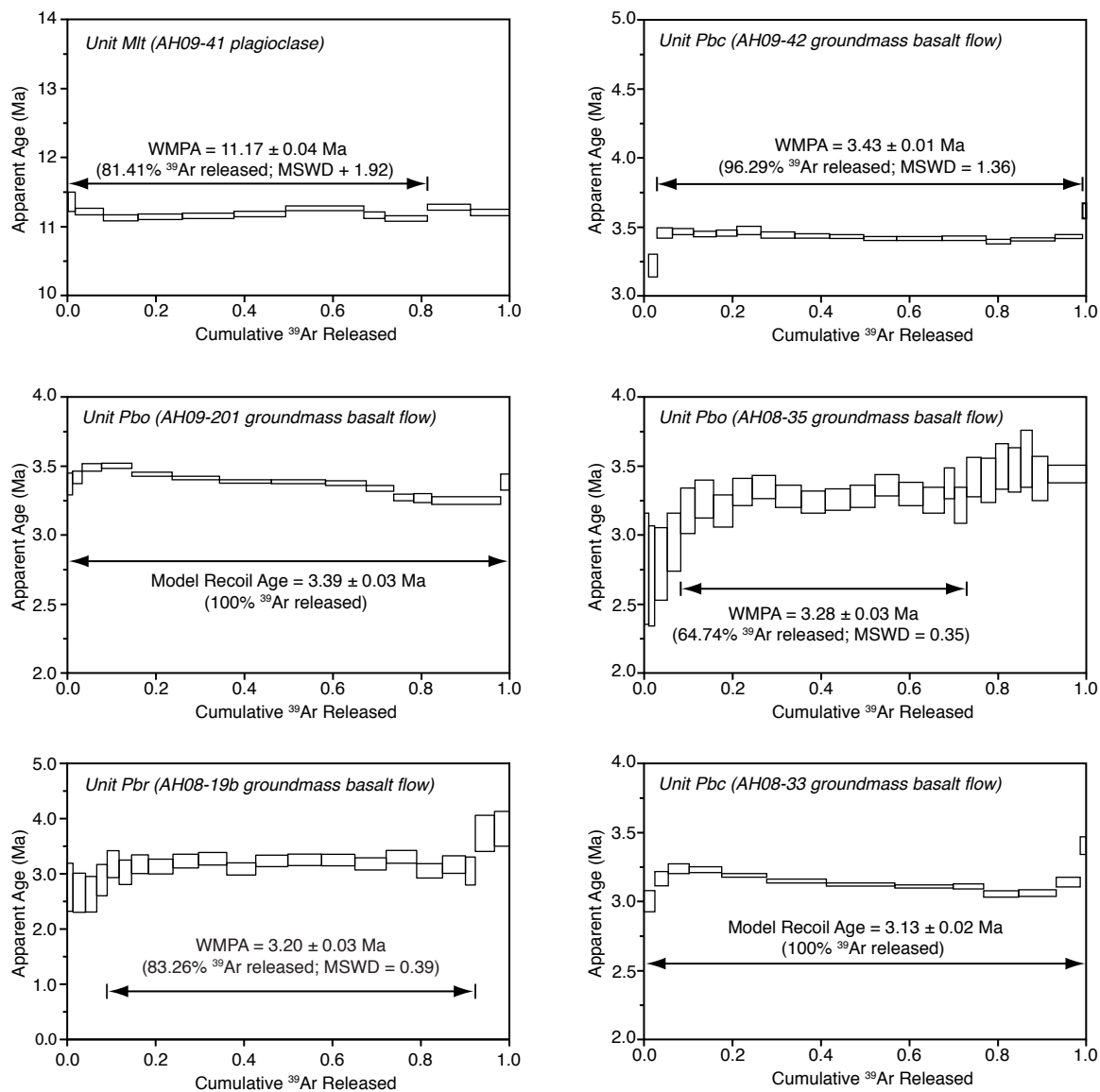


Figure 7. Age spectra for plagioclase within ignimbrite and groundmass concentrate within basalt flows. Summary of ages is shown in Table 1 and analytical data are listed in Data Repository #.

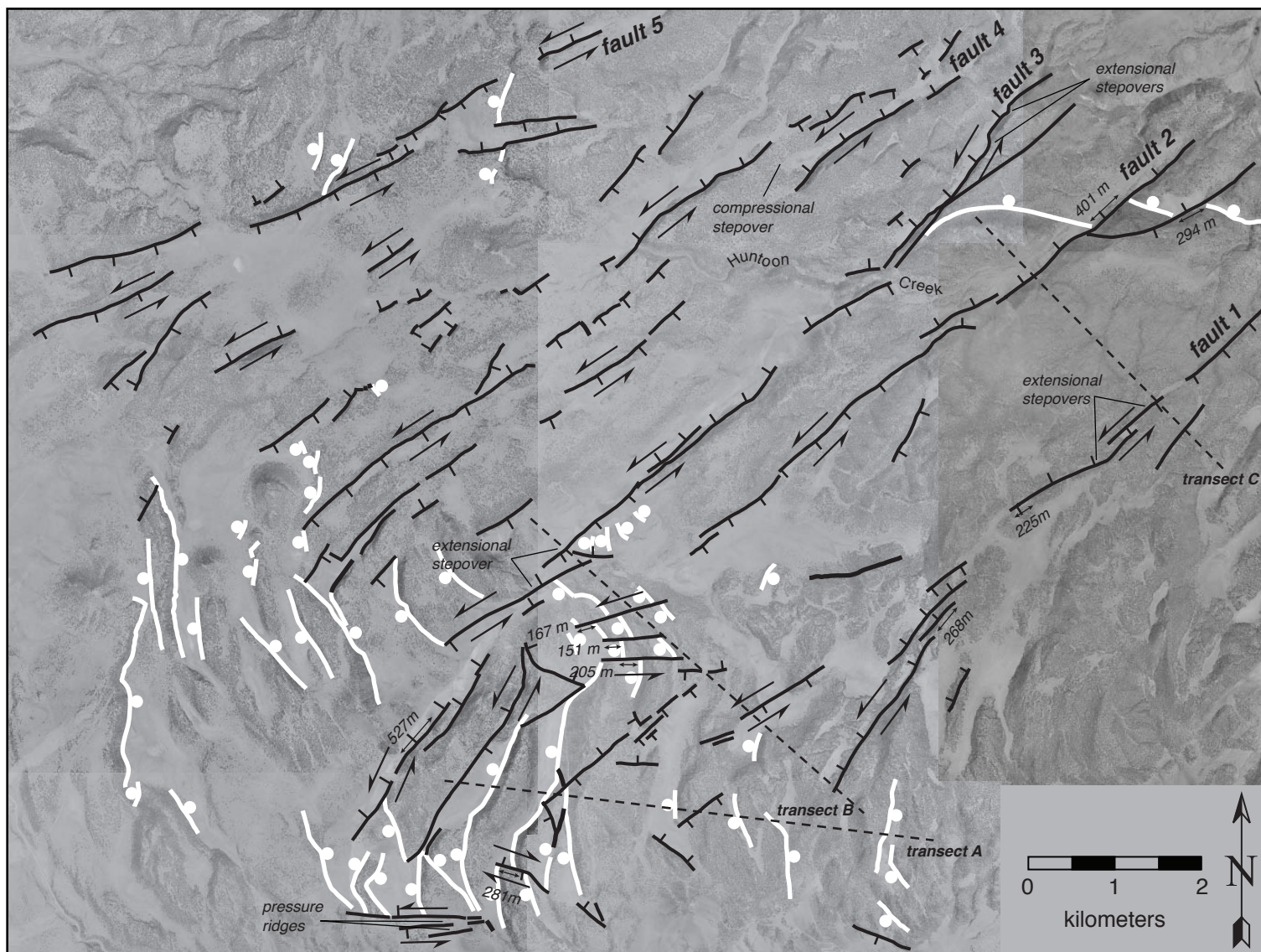


Figure 8. Fault map of the Adobe Hills compiled on digital orthophotographs highlighting primary sinistral fault zones and location of measured lateral offset. Normal faults shown in white; sinistral and dextral faults shown in black. Solid ball, hachures, and paired arrows are defined in Figure 2. See text for discussion of slip calculations along transects.



Figure 9. Field photograph of a playa formed in an extensional step-over or releasing bend along a left-stepping sinistral fault. Paired arrows show relative strike-slip fault motion; solid ball is on the hanging wall of the normal fault. Abbreviations are: Q, undifferentiated Quaternary sediments; Qp, Quaternary playa deposits; and Pb, undifferentiated Pliocene basalts.

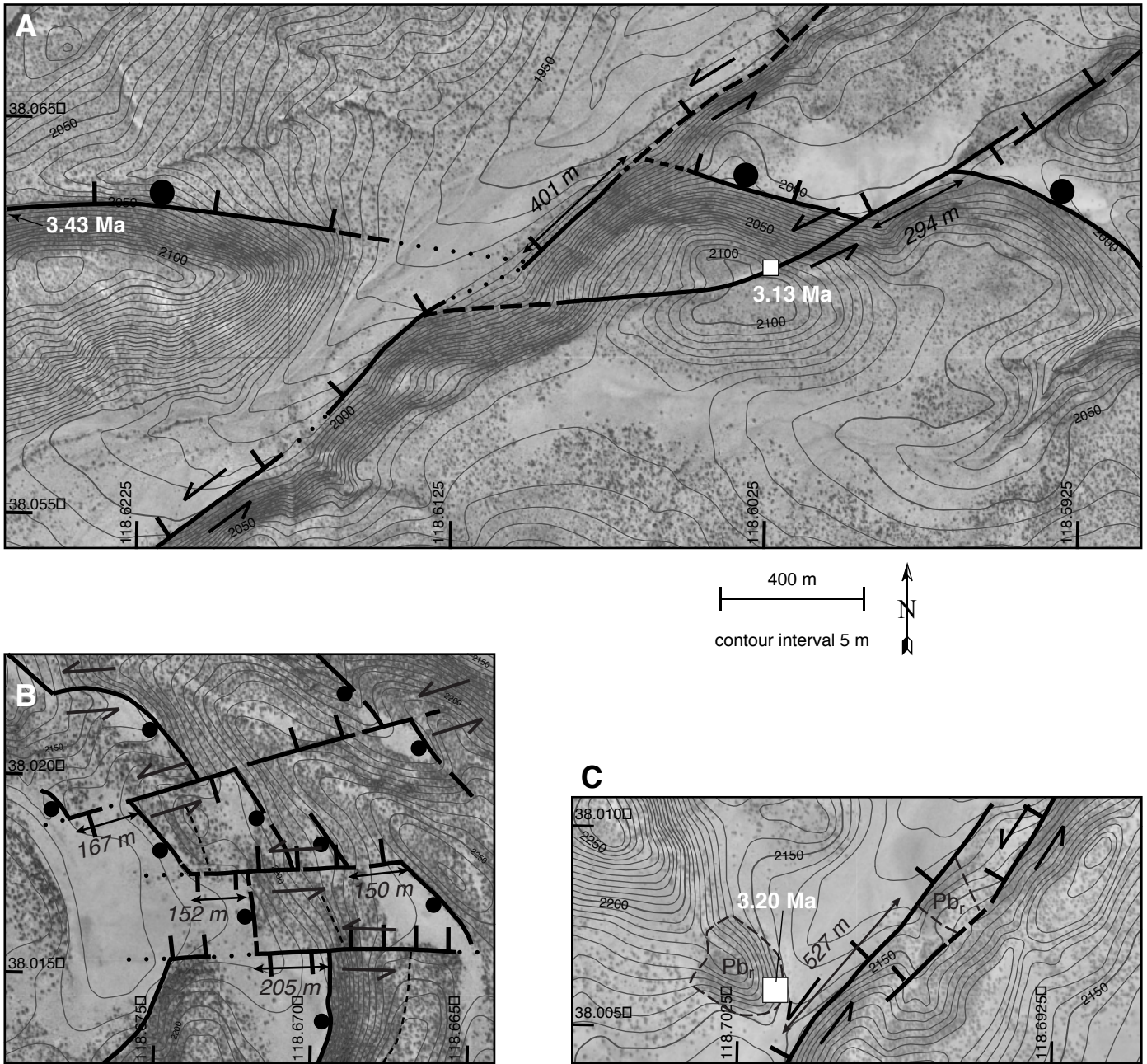


Figure 10. Detailed fault maps superimposed on digital orthophotographs and DEM generated contours showing left lateral offset of geologic features along sinistral faults 2 and 3 (see Figure 8). (A) The intersection line of a normal fault and the surface of its hanging wall basin are sinistrally offset twice for a total of ~695 m along the northeastern segment of fault 2. (B) The southwestern segment of fault 2 is characterized by several subparallel sinistral fault strands that offset the intersection of line of normal faults and hanging wall basins, and a basalt ridgeline (narrow dashed line). The net offset across these sinistral faults is ~523 m. (C) The edge of the basalt rubble flow, unit Pbr, is sinistrally offset ~527 m by fault 3. Paired arrows, solid ball, and hachures are defined in Figure 4, and figure locations are shown in Figure 4.

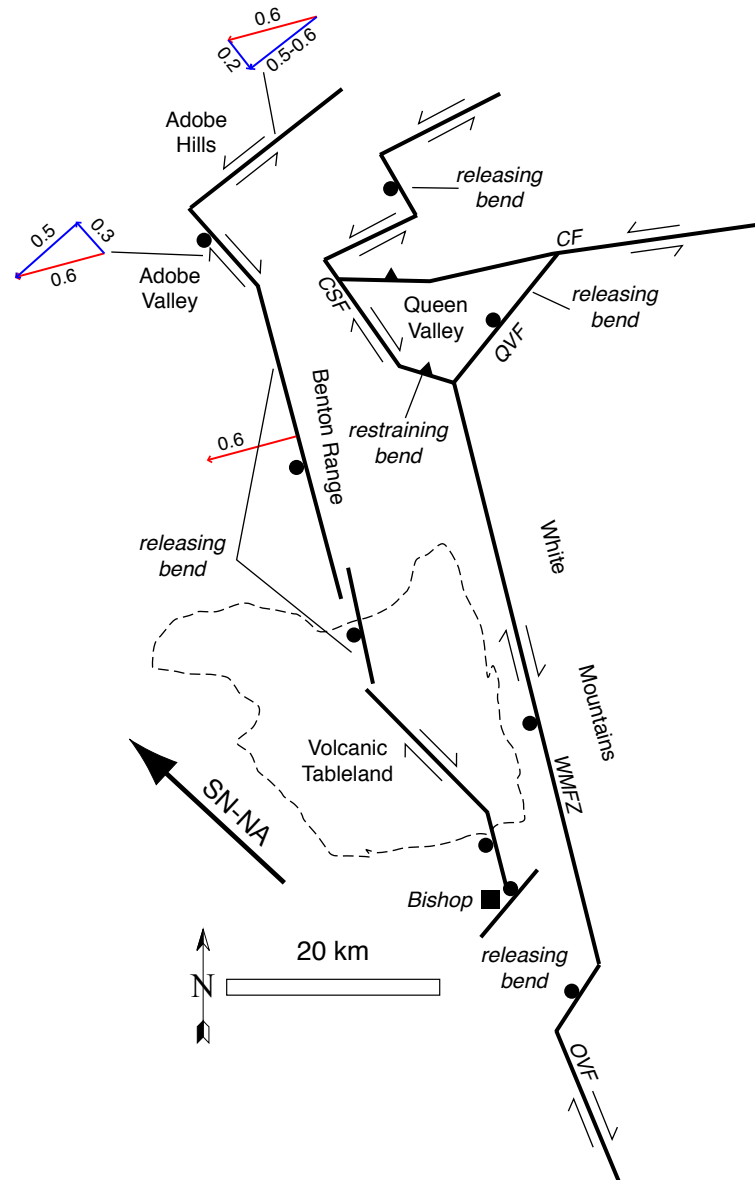


Figure 11. Simplified map highlighting the kinematic link between the Owens Valley fault and sinistral faults in the Adobe Hills. Map shows faults from the Bishop region northward to the Adobe Hills where each major fault or fault zone is shown as a single fault (compare to fault maps in Figs. 2 and 8). Large arrow indicates motion of the Sierra Nevada microplate (SN) with respect to a fixed North American plate (NA) (Dixon et al., 2000). Colored arrows with adjacent numbers indicate fault slip vectors and slip rate in mm/yr. Red arrows show the calculated 0.6 mm/yr ENE-WSW extension across the southern part of Adobe Valley (Benton Range and Black Mountain). Blue arrows and adjacent slip rates indicate the partitioning of the 0.6 mm/yr vector into parallel and perpendicular vectors along NW-striking oblique-slip faults in the eastern Adobe Valley and NE-striking sinistral faults in the Adobe Hills. See text for discussion. Solid ball is on the hanging wall of normal faults and paired arrows indicate relative motion across strike-slip faults. Fault abbreviations: CF—Coaldale fault; CSF, Coyote Springs fault; OVF, Owens Valley fault; QVF—Queen Valley fault; WMFZ—White Mountains fault zone.

APPENDIX A

 $^{40}\text{Ar}/^{39}\text{Ar}$ Analytical Techniques

Minimally weathered volcanic rock samples were collected on top of normal and strike-slip fault scarps for $^{40}\text{Ar}/^{39}\text{Ar}$ geochronology. Grey, crystalline portions of lava flow interiors were separated for dating. Basalt samples and one latite ignimbrite were crushed, washed in an ultrasonic bath and sized to 250–350 μm and 250–500 μm , respectively. Dense, clean basalt groundmass was concentrated using a Frantz magnetic separator and by handpicking under a binocular microscope. Plagioclase from the ignimbrite was hand picked and etched in hydrofluoric acid. For irradiation, ~50 mg groundmass samples were packaged in Cu foil and placed in a cylindrical quartz vial, together with fluence monitors of known age and K-glass and fluorite to measure interfering isotopes from K and Ca. The quartz vials were wrapped in 0.5 mm-thick Cd foil to shield samples from thermal neutrons during irradiation. The samples were irradiated for 4 hours in the central thimble of the U.S. Geological Survey TRIGA reactor in Denver, Colorado (Dalrymple et al., 1981). The reactor vessel was rotated continuously during irradiation to avoid lateral neutron flux gradients. Reactor constants determined for these irradiations were indistinguishable from recent irradiations, and a weighted mean of constants obtained over the past 5 years yields $^{40}\text{Ar}/^{39}\text{Ar}_{\text{K}} = 0.000 \pm 0.004$, $^{39}\text{Ar}/^{37}\text{Ar}_{\text{Ca}} = 0.000706 \pm 0.000051$, and $^{46}\text{Ar}/^{37}\text{Ar}_{\text{Ca}} = 0.000281 \pm 0.000009$. TCR-2 sanidine from the Taylor Creek Rhyolite with an age of 27.87 Ma (Duffield and Dalrymple, 1990) was used as a fluence monitor. This monitor is a secondary standard calibrated against the primary intralaboratory standard, SB-3, that has an age of 162.9 ± 0.9 Ma (Lanphere and Dalrymple, 2000). Data in this study were recalculated to a Fish Canyon sanidine age of 28.02 using $R = 1.00655217 \pm 0.0005853$. Fluence monitors were analyzed using a continuous CO_2 laser system and mass spectrometer described by Dalrymple (1989). Argon was extracted from groundmass and plagioclase using a Mo crucible in a custom resistance furnace modified from the design of Staudacher et al. (1978) attached to the above mass spectrometer. Heating temperatures were monitored with an optical fiber thermometer and controlled with an Accufiber Model 10 controller. Gas was purified continuously during extraction using two SAES ST-172 getters operated at 4A and 0A.

Mass spectrometer discrimination and system blanks are important factors in the precision and accuracy of $^{40}\text{Ar}/^{39}\text{Ar}$ age determinations of young lavas because of low radiogenic yields. Discrimination is monitored by analyzing splits of atmospheric Ar from a reservoir attached to the extraction line. Typical system blanks including mass spectrometer backgrounds were 1.5×10^{-18} mol of m/z 36, 9×10^{-17} mol of m/z 37, 3×10^{-18} mol of m/z 39 and 1.5×10^{-16} mol of m/z 40, where m/z is mass/charge ratio.

In the incremental-heating experiments, the extraction line is isolated from pumping systems, and the sample is heated to a specified temperature for 10 minutes, cooled for 3-5 minutes, and transferred to an isolated mass spectrometer. The gas is exposed to getters during the entire extraction. Isotopic ratios are measured and corrected for instrumental blanks, mass discrimination and interfering isotopes generated in the reactor. In these experiments we separated and loaded enough material to do 12 to 18 steps on each unknown in order to carefully characterize the argon release. The incremental heating data are plotted both as an age spectrum

diagram and as an isotope correlation (isochron) diagram. For the age spectrum, apparent ages are calculated assuming that non-radiogenic Ar is atmospheric ($^{40}\text{Ar}/^{36}\text{Ar} = 295.5$) in composition and are plotted against the cumulative ^{39}Ar released during the experiment. In cases with several contiguous steps yielding ages within analytical error, we calculate and report plateau ages by weighting individual ages by the inverse of their analytical error. Most groundmass age experiments do not yield identical ages across the entire spectrum due to minor alteration, recoil of ^{39}Ar during irradiation or modest excess ^{40}Ar . Generally accepted criteria for a meaningful incremental heating age are: (1) well-defined plateau (horizontal age spectrum) for more than 50% of the ^{39}Ar released; (2) well-defined isochron for the plateau gas fractions; (3) concordant plateau and isochron ages; and (4) $^{40}\text{Ar}/^{36}\text{Ar}$ isochron intercept not significantly different from 295.5.

For isochron plots, data are not corrected using an atmospheric ratio. Isochron ages include plateau steps on well-behaved samples or a subset of data that yield a reasonable goodness of fit. We show normal isochron plots for these low-radiogenic rocks because the data are easier to visualize. Inverse isochron results are indistinguishable. The most reliable results generally include gas from the middle of the release spectrum with consistent K/Ca ratios and concordant isochron data with $^{40}\text{Ar}/^{36}\text{Ar}$ intercepts within error of air.

Target atoms recoil upon conversion from potassium or calcium to argon. Recoil distances have been measured at $\sim 0.08 \mu\text{m}$ for ^{39}K to ^{39}Ar and are estimated to be longer for ^{40}Ca to ^{37}Ar . Groundmass concentrates from lavas often have fine textures and argon recoil significantly redistributes these isotopes and affects isotopic ratios. "Recoil ages" are attempts to correct for recoil by weighting discordant apparent ages by their ^{39}Ar released and their dispersion. Ages and isotopic ratios reported are 1σ .

